Politecnico di Torino

Department of Mechanical and Aerospace Engineering

Master's Degree in Mechanical Engineering LM-33

Dynamic Analysis of the Dynamill G5 gantry milling machine Using Simulation and Experimental Approaches

Supervisors:

Prof. Alessandro Fasana

Eng. Manuel Lepori

Candidate:

Reza Rahmani

Accademic Year
2023/2024

Contents

1 Introduction **2**

1.1 Overview of CNC Machining 2

1.2 Importance of Dynamic Analysis 2

1.3 Objectives of the Thesis 3

2 Literature Review **5**

2.1 Review of Machine Tool Dynamics 5

2.1.1 Dynamic Behavior of CNC Machine Tools 5

2.1.2 Adverse Effects of Chatter 9

2.1.3 Interaction Between Cutting Forces and Vibrations in Machining Processes 14

2.1.4 3D Force Model in Machining 16

2.1.5 Regenerative Chatter, Stability Criterion, and Feedback Loops in Milling Operations 19

2.1.6 Stability Regions and Instability 22

2.1.7 Stability Lobe Diagram Analysis 24

2.1.8 Dynamic Cutting Forces in Milling 25

2.2 Previous research on chatter and machine stability 27

2.2.1 One Degree of Freedom Theories 28

2.2.2 Two Degrees of Freedom Theories 30

2.2.3 Critical Analysis of Research Gaps 34

3 Methodology **36**
3.1 Description of the Dynamill G5 Gantry Milling Machine 36
3.2 Simulation Tools and Techniques 38
3.2.1 Static Analysis 38
3.2.2 Modal Analysis 39
3.3 Experimental Setup and Procedures 40
3.3.1 Experimental Procedure 40
3.4 Stability Lobe Diagram Computation Using MillingStab Software 42
3.4.1 Initial Setup and Input Parameters 43
3.4.2 FRF Insertion and Stability Analysis 43

4 Results and Discussion **45**
4.1 EMA Results 46
4.2 Mode Identification Analysis 48
4.2.1 EMA Analysis 48
4.2.2 FEM Analysis 51
4.2.3 Comparison of EMA and FEM Analyses 53
4.3 Frequency Response Functions 55
4.3.1 EMA Analysis 55
4.3.2 FEM Analysis 59
4.3.3 Comparison of EMA and FEM Analyses 60
4.4 Stability lobe diagrams 61
4.4.1 Analysis of Stability Lobe Diagrams Derived from EMA-Based FRFs 65
4.4.2 Analysis of Stability Lobe Diagrams Derived from FEM-Based FRFs 68
4.4.3 Comparison of EMA and FEM Stability Lobe Diagrams 70

5 Conclusion and Future Works **71**
5.1 Conclusion 71
5.2 Future Works 73

6 Appendix **75**

List of Figures

2.1 Types of vibrations in machining: free vibration, forced vibration, and self-excited vibration (chatter)[Moreau (2010)]. 6
2.2 Photo of a machining pass taken to highlight temporary instabilities at the entry (right) and exit (left) of the workpiece [Moreau (2010)]. 8
2.3 Comparison of Cutting Forces During Normal Machining and Machining with Vibration 10
2.4 Tool Wear Due to Chatter 11
2.5 Workpiece surface finishing: (a) chatter; (b) no chatter. 12
2.6 Simulated bearing contact forces under cutting (spindle speed:6000 rpm, feed rate: 0.1 mm/flute)[Yuzhong Cao and Y. Altintas (2007)]. 13
2.7 Interaction between cutting forces and tool vibrations in machining . . . 14
2.8 Comparison of tool movement in turning: (A) Longitudinal turning (Z direction) and (B) Radial turning (X direction). 15
2.9 Turning process showing tool feed, rotation, and key parameters like depth of cut and chip thickness 16
2.10 Orthogonal and oblique cutting geometries. The three primary force components in the oblique cutting model: Tangential (F_t), Radial (F_r), and Axial (F_a). 17
2.11 Illustration of force components in the 3D force model for milling operations. 18
2.12 Control system representation of regenerative chatter in milling operations. 20
2.13 Stability and instability regions based on the ratio between the natural frequency f_n and the tooth-passing frequency f_t. 23

2.14 Stability lobe diagram showing the relationship between axial depth of cut and spindle speed. 24
2.15 The interaction between cutting forces and tool vibrations. 25
2.16 Schematic Representation of End Mill Cutter in Milling Operation 26
2.17 Influence of Present and Previous Dynamic Displacements in Milling Operations 27
2.18 Regeneration of Waviness in Turning [Tlusty (1986)] 29
2.19 Deriving Stability Lobes[Tlusty (1986)] 29
2.20 Dynamic model of milling with two degrees of freedom [Altintas and Budak] 31
2.21 Theoretical model of asymmetrical boring bar of a coupled system [Celikag, Ozturk, and Sims]. 33

3.1 Overall dimensions & Working Envelope of the Gantry Milling Machine Dynamill G5 36
3.2 Stiffness properties of (A) the rack-and-pinion connection, (B) upper support, and (C) lower support. 38
3.3 Experimental Modal Analysis Setup Schematic 41
3.4 Analysis of MIF, FRFs, Coherence, and Modal Circles in Dewesoft-X-PROF 42
3.5 Detailed View of the Process Definition Section 43
3.6 Stability Lobes Diagram Calculation 44

4.1 The setup for data acquisition. 46
4.2 Frequency Response Analysis of the Machine Tool with force applied in X direction. 47
4.3 Frequency Response Analysis of the Machine Tool with force applied in Y direction. 47
4.4 MIF (Mode Indicator Function) plot 49
4.5 Magnitude and Phase plot of FRF for Different Directions 49
4.6 Mode shape visualization at 24.3 Hz generated in DewesoftX software. . . 50
4.7 Mode shape visualization at 300.1 Hz generated in DewesoftX software. . 51

4.8 Heatmap illustrating the correlation metric between EMA and FEM modes. 53
4.9 Comparison of normalized FRF magnitudes for EMA Mode 1 and FEM Mode 6 in the X, Y, and Z directions. 54
4.10 Displacement-on-Force Frequency Response Functions for the X, Y, and Z directions with force applied in the X direction. 56
4.11 Displacement-on-Force Frequency Response Functions for the X, Y, and Z directions with force applied in the Y direction. 57
4.12 FEM-Generated FRFs with Force Applied in the X Direction 59
4.13 FEM-Generated FRFs with Force Applied in the Y Direction 60
4.14 345 Face Milling Cutter technical illustrations 62
4.15 Illustration of radial depth of cut (AE) and engagement angle (θ) in milling 63
4.16 Input parameters entered in the MillingStab software for lobes diagram computation, including cutting force coefficients, start/exit angles, and rotation direction, with FRFs yet to be selected. 65
4.17 Stability Lobe Diagram with XX-XY FRFs (EMA-Based). 66
4.18 Stability Lobe Diagram with XX-YY FRFs (EMA-Based). 67
4.19 Updated Stability Lobe Diagram with YY-XY FRFs (EMA-Based). . . . 67
4.20 Updated Stability Lobe Diagram with XX-XY FRFs (FEM-Based). . . . 68
4.21 Updated Stability Lobe Diagram with XX-YY FRFs (FEM-Based). . . . 69
4.22 Updated Stability Lobe Diagram with YY-XY FRFs (FEM-Based). . . . 69

List of Tables

4.1 Modal frequencies obtained from FEM 52
4.2 CoroMill® 345 Face Milling Cutter Specifications 62
4.3 Input Parameters for Lobes Diagram Computation 64

6.1 ICP® Impact Hammer Specifications (Model TLD086C04) 76
6.2 Triaxial ICP® Accelerometer Specifications (Model 356A45) 77
6.3 CoroMill® 345 Face Milling Cutter Specifications 78

Abstract

The dynamic behavior of CNC machine tools plays a crucial role in determining their performance, stability, and machining precision. This thesis investigates the dynamic performance of the Dynamill G5 gantry milling machine, integrating simulation and experimental methods to evaluate and optimize its operational stability. The research begins with the development of a Finite Element Model (FEM) in CATIA V5, providing insights into the machine's structural characteristics, including Frequency Response Functions (FRFs), mode shapes, and stability lobe diagrams. Complementing this, Experimental Modal Analysis (EMA) was conducted using impact testing to assess the machine's dynamic compliance, damping ratios, and resonance frequencies under real-world conditions.

The findings reveal significant anisotropic stiffness in the Dynamill G5, with higher compliance in the X direction and greater stiffness along the Y axis. A comparative analysis between FEM and EMA highlights discrepancies in resonance frequencies and stability predictions, underscoring the necessity of experimental validation to refine simulation-based models. Stability lobe diagrams were generated using the MillingStab software, leveraging both FEM- and EMA-derived FRFs. The results demonstrated that EMA provides more accurate stability predictions due to its incorporation of real-world damping and spindle-tool interactions, while FEM serves as a valuable preliminary tool for design optimization.

This research contributes a robust framework for analyzing and enhancing the dynamic performance of CNC machine tools, combining theoretical modeling with experimental validation. Recommendations for future work include improved FEM modeling with realistic damping parameters, multi-axis experimental analysis, and the integration of real-time stability monitoring systems to further advance machining precision and reliability.

Acknowledgments

I would like to express my deepest gratitude to everyone who supported me throughout this thesis journey.

My heartfelt thanks go to my academic advisor, Professor Fasana, for their invaluable guidance and mentorship. I am equally grateful to Manuel Lepori, my supervisor at MECOF company, as well as Simone Roati and Alessandro Paolo Daga, for their expertise and assistance, which greatly enriched my research.

I extend my sincere appreciation to MECOF company for providing the resources and financial support necessary for this work, and to Politecnico di Torino for its academic environment and facilities.

Finally, I am forever thankful to my family, whose belief in me inspired this journey abroad, and to my beloved girlfriend, whose unwavering support was essential in completing this milestone.

Reza Rahmani
Politecnico di Torino
December 2024

Chapter 1

Introduction

1.1 Overview of CNC Machining

Computer Numerical Control (CNC) machine tools are integral to modern manufacturing processes, facilitating high-precision machining in sectors such as aerospace, automotive, and electronics. CNC machines utilize computer systems to automate the control of machining tools, which enhances the accuracy and efficiency of production. The dynamic behavior of these machines, including their vibrational response and inherent damping capacity, significantly influences not only the quality of the machined components but also tool longevity and overall productivity. Understanding the operational dynamics of CNC machines is essential for optimizing machining performance and extending the useful life of cutting tools.

1.2 Importance of Dynamic Analysis

The dynamic analysis of CNC machine tools is vital for assessing their performance and stability. Variations in the dynamic characteristics of the machine, such as its natural frequencies and damping ratios, can lead to undesirable phenomena like chatter, which adversely affects machining accuracy and surface finish. By evaluating the dynamic

behavior of CNC machines, engineers can identify potential stability issues and optimize cutting parameters to mitigate these challenges. Furthermore, dynamic analysis provides insights into the machine's response to external forces during operation, allowing for enhanced design modifications and improved operational strategies.

1.3 Objectives of the Thesis

The primary objective of this thesis is to investigate and analyze the dynamic performance of the Dynamill G5 gantry milling machine, focusing on improving its operational stability and structural resilience. Achieving this goal requires a combination of simulation and experimental methods to accurately assess and optimize the machine's dynamic behavior. The specific objectives of this research are as follows:

1. **Develop a Finite Element Model:**
   To create a detailed finite element model (FEM) of the Dynamill G5 using CATIA V5, enabling a comprehensive analysis of the machine's structural dynamics. This model aims to capture critical dynamic responses, including Frequency Response Functions (FRF), mode shapes, and stability lobes.

2. **Conduct Experimental Modal Analysis (EMA):**
   To perform Experimental Modal Analysis using impact testing, which involves an instrumented hammer and accelerometers to evaluate the real-life dynamic compliance, damping, and resonance frequencies of the machine. This experimental data serves as a baseline for understanding the machine's in-situ dynamic behavior.

3. **Correlate Simulation and Experimental Results:**
   To compare the outcomes from the FEM and EMA to assess the accuracy and reliability of the simulation model. This objective includes identifying consistencies and discrepancies in key parameters such as Frequency Response Functions, mode shapes, and stability lobes, allowing for a deeper understanding of the machine's dynamic performance and potential areas for optimization.

4. **Validate Stability in Milling Operations:**
   To validate the machine's stability under operational conditions by conducting milling tests based on the predicted stability boundaries. This objective ensures the reliability of the machine's performance under dynamic forces encountered during milling, contributing to enhanced machining precision and reduced wear.

These objectives aim to provide a well-rounded assessment of the Dynamill G5's dynamic characteristics, offering both theoretical insights and practical recommendations for enhanced milling performance and stability.

Chapter 2

Literature Review

2.1 Review of Machine Tool Dynamics

2.1.1 Dynamic Behavior of CNC Machine Tools

In high-precision machining, such as Computer Numerical Control (CNC) operations, dynamic instabilities significantly impact the quality and efficiency of material removal processes. Among the primary factors influencing this dynamic behavior are vibrations, particularly forced vibrations and self-excited vibrations, commonly referred to as chatter. These phenomena are crucial considerations in the dynamic analysis of CNC machine tools, as they affect surface quality, tool wear, and the overall stability of the process.
Vibration issues in machining have been present since the early 20th century. In 1907, Frederick W. Taylor mentioned chatter in machining as one of the most challenging issues to address. Throughout the 20th century, According to Moreau (2010)[1], three types of vibrations occur during a machining operation: **free vibrations**, **forced vibrations**, and **self-excited vibrations**. These three categories are detailed in this section and illustrated in Figure 2.1

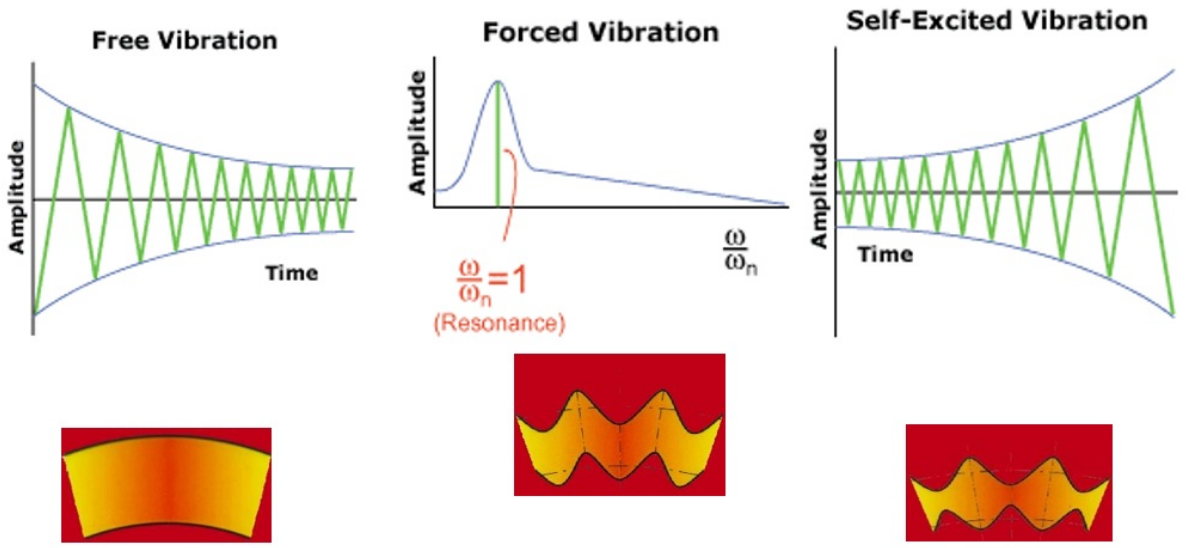

Figure 2.1: Types of vibrations in machining: free vibration, forced vibration, and self-excited vibration (chatter)[Moreau (2010)].

Free Vibrations

They correspond to the natural vibrational response of any mechanical system to a brief excitation, such as an impact. Due to the natural damping present in all mechanical systems, the amplitude of these oscillations decays over time. This phenomenon is represented by an exponentially decaying wave, where the amplitude decreases gradually to zero. In milling, free vibration leads to minimal influence on the surface quality, resulting in a relatively smooth finish as shown in Figure 2.1 and they are generally used for system characterization, during a hammer test.

Forced Vibrations

Forced vibration in machining occurs when an external periodic force, such as a fluctuating cutting load, interacts with the system. If this force's frequency aligns with the system's natural frequency, resonance amplifies vibration amplitude, posing risks like

excessive tool wear and machine damage. This resonance effect also impacts surface quality by introducing periodic undulations on the finish. As depicted in Figure 2.1, chip thickness displays a consistent "in-phase" wave pattern aligned with these external forces. Although forced vibrations do not destabilize the process, they create a wavy surface profile that may affect product quality.

In machining contexts, forced vibrations arise from periodic excitation, meaning that the cutting tool intermittently engages with the material. This phenomenon is particularly evident in milling, where cutting forces intermittently stress the tool's teeth, generating forced vibrations. To mitigate these effects, achieving near-continuous cuts is beneficial. Research by Patel [2] and Campomanes [3] has shown that cutting continuity can be optimized using high helix angle tools or adjusting parameters like radial immersion, feed per tooth, or depth of cut.
This type of vibration can also occur in the case of turning a non-cylindrical part. Here, variation in the depth of cut over a revolution, as in milling, leads to fluctuating forces, thereby exciting the tool with forced vibrations. Peigné [4] and Albrecht [5] introduce other possible sources of forced vibrations, such as:

- Material heterogeneities.
- Geometrical irregularities of the workpiece.
- Runout and imbalance effects; Schmitz [6] studied these effects on surface quality and stability.
- Excessive wear or breakage of a tooth in milling.

Although secondary compared to cutting irregularities, these factors should not be overlooked under certain circumstances, such as:

- A high-speed rotating tool in milling.
- A part deformed by clamping in turning, as studied by Jeong [7].

These vibrations have a relatively low impact on surface quality as they match the tooth-passing frequency. Consequently, with each tool revolution, material removal is consistent, avoiding irregularities in machining. However, upon tool entry or exit from the material, when steady-state conditions are not yet established, the combination of free vibrations (due to tool impact on the material) and forced vibrations (due to tool rotation) often results in vibrations, as shown in Figure 2.2.

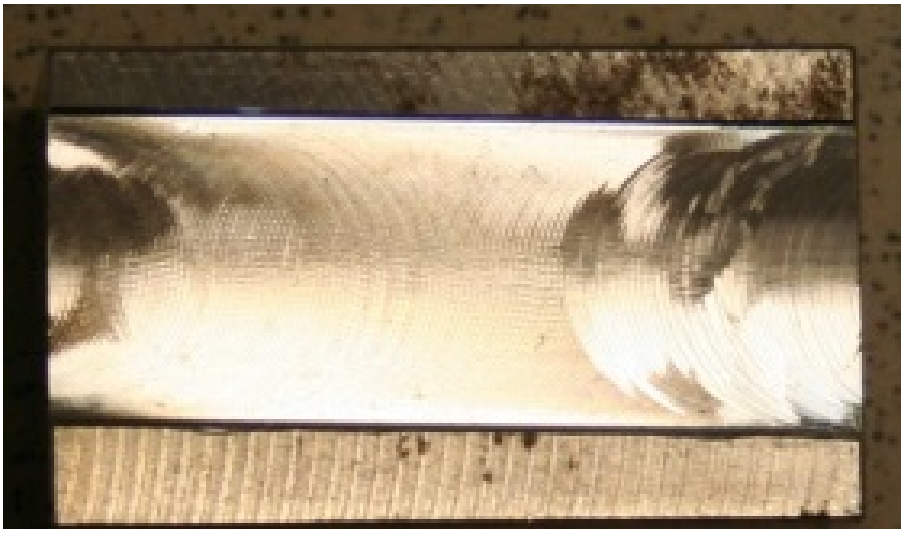

Figure 2.2: Photo of a machining pass taken to highlight temporary instabilities at the entry (right) and exit (left) of the workpiece [Moreau (2010)].

Self-Excited Vibrations (Chatter)

Self-excited vibrations, or chatter, are unstable, self-sustaining vibrations that arise from the interaction between the cutting process and the tool structure. Unlike free or forced vibrations, chatter can escalate over time, increasing vibration amplitude significantly. This occurs as each tooth pass amplifies the vibration through regenerative feedback, leading to an "out-of-phase" chip formation and producing a rough, irregular surface finish, as shown in 2.1. Chatter is especially problematic in milling, reducing tool life, degrading surface quality, and potentially damaging both the workpiece and machine.

Self-sustained vibrations emerge during a transition from a stable to an unstable cut-

ting regime, where the system vibrates at a frequency distinct from the tooth-passing frequency. This dynamic shift, known as chatter, signifies a critical point in the machining process and is highly detrimental as it generally results in:

- Poor surface finish on the final workpiece.
- Reduced tool life due to accelerated wear or, in extreme cases, tool breakage.
- A very unpleasant noise during machining, which, though it does not affect the quality of the final part, can impact the operator's work environment.
- Premature wear of the machine spindle.

Unlike forced vibrations, chatter produces *out-of-phase waves*, meaning that the vibrations from the previous tool pass interfere destructively with the current pass, causing the amplitude of the oscillations to increase progressively. This regenerative chatter not only deteriorates the surface quality of the workpiece, creating irregular and unstable chip formation, but it also significantly reduces tool life and can lead to severe damage to the machine and workpiece. Chatter vibrations are considered highly undesirable as they lead to unstable machining conditions, reduced productivity, and increased operational costs.

These issues were studied in the mid-20th century by researchers such as Arnold [8], Tlusty and Polacek [9], Merritt [10], and Tobias [11] to understand the conditions that lead to chatter and to develop prediction methods. Zhao and Balachandran [12] classify known sources of self-sustained vibrations into two categories: regenerative and non-regenerative.

2.1.2 Adverse Effects of Chatter

Tool Wear and Damage

One of the most immediate and severe impacts of chatter is the accelerated wear or potential damage to the cutting tool. When chatter occurs, the cutting tool experiences

oscillating cutting forces and velocities, resulting in cyclical loading conditions. These oscillations increase the energy dissipation in the form of friction between the tool and the workpiece. As a result, the temperature in the cutting zone rises, exacerbating the wear mechanisms.

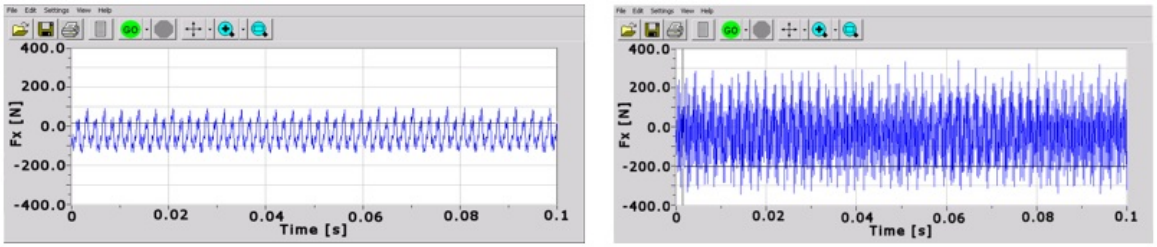

Figure 2.3: Comparison of Cutting Forces During Normal Machining and Machining with Vibration

Friction, combined with repeated impact-like forces from vibration, significantly accelerates the wear process. High temperatures in the cutting zone promote diffusion and adhesion wear, where material from the tool transfers to the workpiece or vice versa, degrading the cutting edge. Over time, this wear can result in tool failure, necessitating more frequent tool changes and increasing production costs. Various studies, such as the works of Tlusty (1986)[13] and Altintas& Budak, (1995)[14], have demonstrated that chatter-induced vibrations lead to nonlinear wear behavior, where wear rates significantly increase once a critical vibration threshold is crossed. The complexity of chatter-induced wear also lies in its irregular nature, often causing localized hot spots on the tool, further intensifying wear at specific points along the cutting edge.

Figure 2.4: Tool Wear Due to Chatter

Surface Finish

Chatter has a direct and detrimental effect on the surface finish of the machined workpiece. As the tool vibrates due to chatter, it oscillates around its intended cutting path. This vibration leads to uneven contact between the tool and the workpiece, particularly with the heel of the tool dragging along the milled surface, which distorts the surface profile. The result is a poor surface finish with ripples, chatter marks, or tool marks, which are visible as a periodic wave pattern on the machined surface.

Surface roughness induced by chatter is often more severe than that caused by stable cutting conditions. In cases where finishing operations are critical, such as aerospace or automotive component manufacturing, this poor surface quality can lead to part rejection or the need for additional machining operations to correct the surface, increasing cycle times and costs.

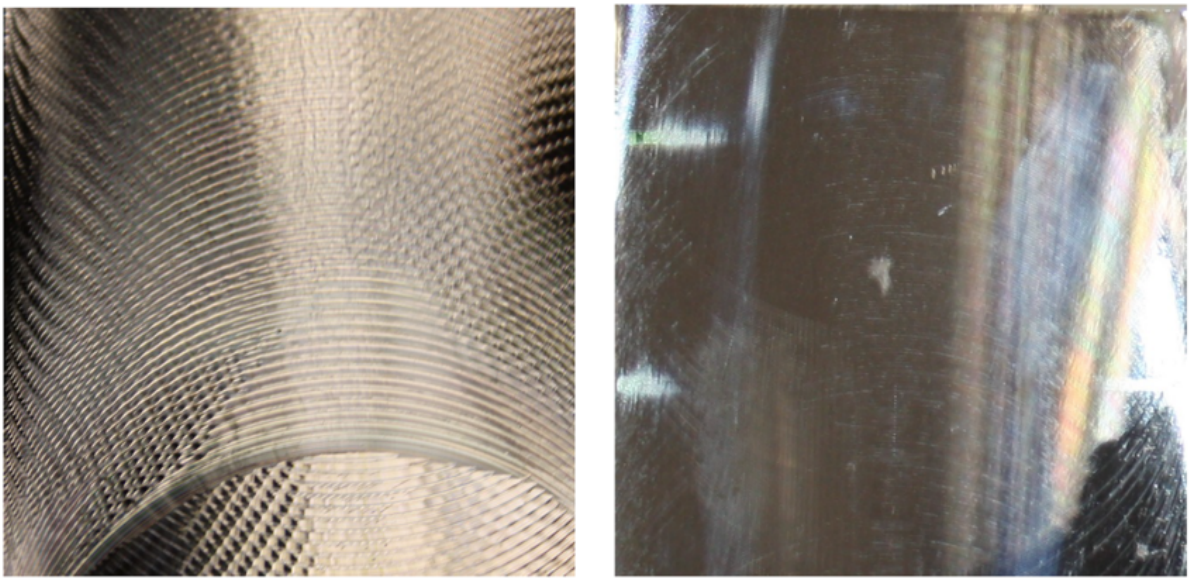

Figure 2.5: Workpiece surface finishing: (a) chatter; (b) no chatter.

Studies by Altintas and Budak (1995) emphasized the detrimental effect of chatter on surface integrity, linking the amplitude of vibrations to specific surface roughness values. Their work underlined that as vibration amplitude increases, the frequency of interaction between the tool and workpiece also increases, leading to worsening surface quality.

Damage to Spindle Bearings

Spindle bearings are another critical component adversely affected by chatter. The oscillating forces and vibrations induced by chatter propagate through the cutting tool and into the spindle assembly. Over time, these vibrations can cause wear and fatigue in the spindle bearings. The high-frequency vibrations impose cyclical stresses on the bearing components, potentially leading to premature failure.

Bearing failure due to chatter not only reduces machine tool accuracy but also requires costly maintenance and repairs. The long-term health of a CNC machine can be significantly compromised if chatter is not controlled, leading to reduced spindle life and higher machine downtime.

Research conducted by Yuzhong Cao and Y. Altintas (2007)[15] has emphasized the critical role of spindle bearing performance in ensuring machining precision and reliability. They highlighted how spindle bearings are subjected to significant dynamic loads during cutting operations, which can lead to damage over time. Figure 2.6, which presents the simulated bearing contact forces under cutting conditions (spindle speed: **6000 rpm**, feed rate: **0.1 mm/flute**), demonstrates the distribution and magnitude of these forces within the spindle-bearing system. The authors suggest that excessive bearing contact forces, as illustrated in this figure, can result in detrimental effects, such as increased wear, reduced bearing lifespan, and eventual failure, all of which compromise the overall performance of the machine tool. This insight underscores the importance of optimizing spindle design and cutting conditions to mitigate bearing damage and enhance system durability.

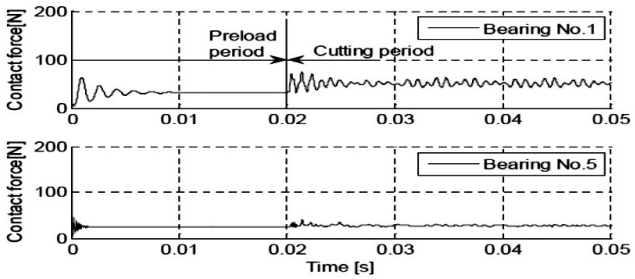

(a) Simulated bearing contact forces under cutting (DOC=2mm, no chatter)

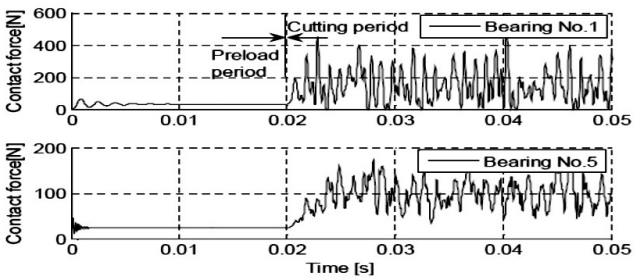

(b) Simulated bearing contact forces under cutting (DOC=4mm, chatter)

Figure 2.6: Simulated bearing contact forces under cutting (spindle speed:6000 rpm, feed rate: 0.1 mm/flute)[Yuzhong Cao and Y. Altintas (2007)].

2.1.3 Interaction Between Cutting Forces and Vibrations in Machining Processes

One of the critical factors in the dynamic behavior of machining processes, particularly in turning and milling operations, is the interaction between cutting forces and vibrations. The cutting process is highly dependent on the relative motion between the cutting tool and the workpiece, which directly influences the geometry and thickness of the chip being formed. The cutting force influences tool vibrations through the machine's frequency response (displacement/force), while tool vibrations, in turn, affect the cutting process by modifying chip formation, tool geometry, and material interaction. This creates a regenerative feedback loop, where vibrations can amplify over time, leading to dynamic instability in the machining process, such as chatter.

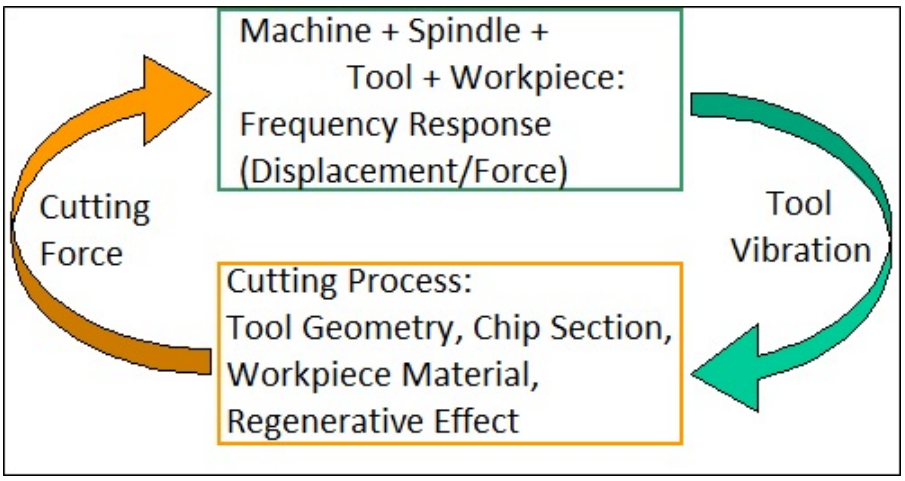

Figure 2.7: Interaction between cutting forces and tool vibrations in machining

In typical turning operations, the cross-section of the chip is a thin rectangular shape. Vibrations occurring along the shorter side of this rectangle, corresponding to the chip thickness, result in significant variations in the chip cross-section. These variations are especially pronounced when the oscillations are in the direction of the cutting force, contributing to dynamic instability in the machining process.

There are two primary types of turning operations affected by such interactions:

- **Longitudinal Turning**: In this process, the tool moves in the axial (Z) direction of the workpiece, producing a continuous chip. This type of motion is highly sensitive to vibrations that can cause deviations in chip thickness, leading to surface defects or chatter.
- **Radial Turning (Facing)**: In radial turning, the tool moves in the X direction, and similar vibrations can affect the chip thickness, particularly at the beginning and end of the tool pass.

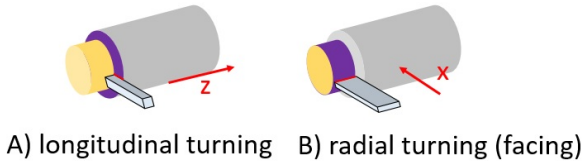

Figure 2.8: Comparison of tool movement in turning: (A) Longitudinal turning (Z direction) and (B) Radial turning (X direction).

Researchers have developed various models to understand the mechanics of chatter and predict its onset. One key approach is modeling the cutting force as a function of the instantaneous chip thickness, expressed as:

$$F_{\text{cut}} = K \cdot a \cdot h$$

where:

- K is a material-dependent constant representing the cutting force coefficient,
- a is the width of the cut, and
- h is the instantaneous chip thickness.

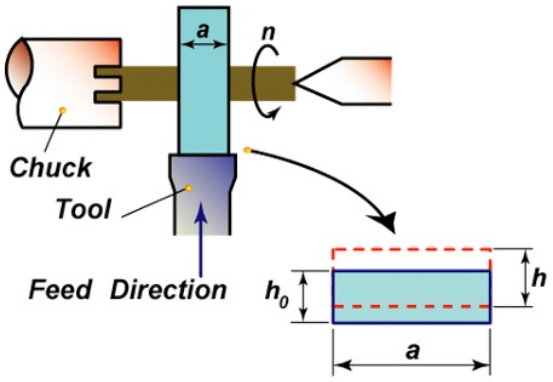

Figure 2.9: Turning process showing tool feed, rotation, and key parameters like depth of cut and chip thickness

The proportional relationship between cutting force and chip thickness underscores the need to minimize vibrations to ensure a stable and consistent cutting process. Excessive tool vibrations result in irregular chip formation, which can ultimately lead to chatter. Researchers have emphasized the critical role of controlling vibrations in machining systems, particularly through optimizing cutting parameters and tool geometry, as well as through advanced machine tool designs that aim to minimize structural deformations and enhance damping capabilities. By reducing the impact of these oscillations, it is possible to improve the overall quality and productivity of machining operations, while avoiding detrimental effects such as chatter, which is often caused by the regenerative effect described earlier.

2.1.4 3D Force Model in Machining

The force model in machining processes is essential for understanding the dynamic behavior of cutting tools and workpieces, particularly in milling operations. In the 3D force model, both orthogonal and oblique cutting geometries are considered to account for the complexity and realism of the machining forces involved.

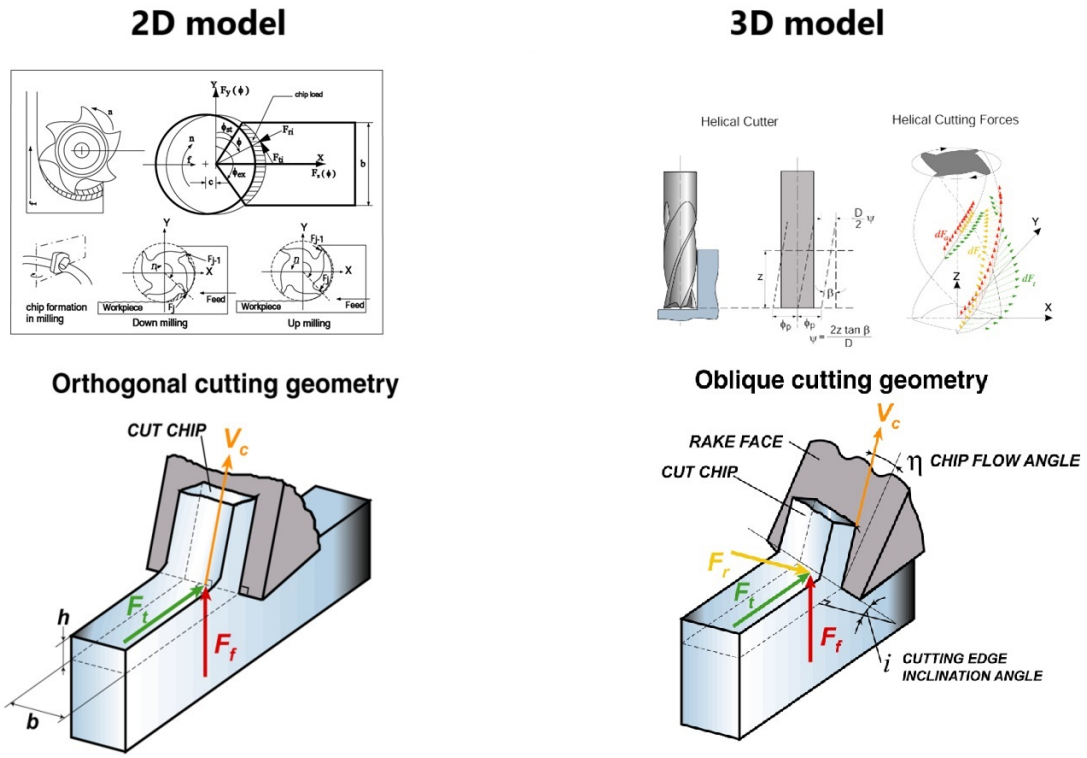

Figure 2.10: Orthogonal and oblique cutting geometries. The three primary force components in the oblique cutting model: Tangential (F_t), Radial (F_r), and Axial (F_a).

Orthogonal and Oblique Cutting Geometries

In the orthogonal cutting model, the cutting forces are simplified to two main components acting on the tool. However, in reality, milling operations are more accurately described using a 3D oblique cutting model where forces act in multiple directions, making it necessary to decompose them into three primary force components:

- **Tangential Force** (F_t)
- **Radial Force** (F_r)
- **Axial Force** (F_a)

Equations for Force Components and Parameters in MillingStab

The tangential, radial, and axial forces in a milling operation can be expressed as follows:

$$F_t = F_{tc} + F_{te} = K_{tc}\, b\, h + K_{te}\, b$$

$$F_r = F_{rc} + F_{re} = K_{rc}\, b\, h + K_{re}\, b$$

$$F_a = F_{ac} + F_{ae} = K_{ac}\, b\, h + K_{ae}\, b$$

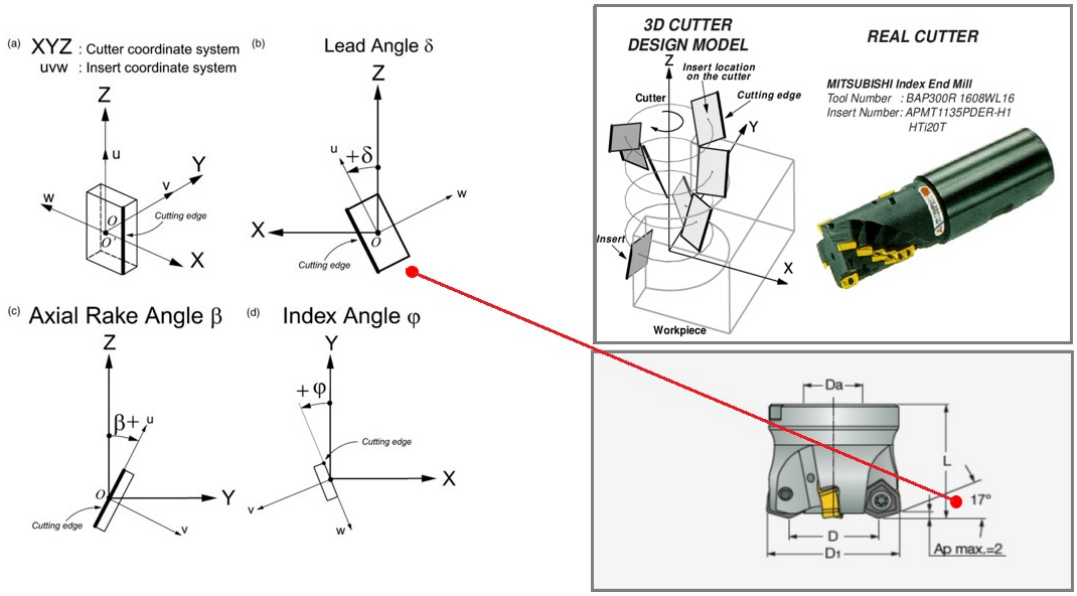

Figure 2.11: Illustration of force components in the 3D force model for milling operations.

where:

- $K_{tc}, K_{te}, K_{rc}, K_{re}, K_{ac}, K_{ae}$ are the cutting force coefficients.
- b is the depth of cut.
- h is the undeformed chip thickness.

Calculation of Axial and Radial Cutting Force Coefficients

In the first approximation, the axial cutting force coefficient K_{ac} can be calculated from the tangential cutting force coefficient K_{tc} and the radial cutting force coefficient K_{rc} as follows:

$$K_{ac} = K_{rc_0} \cdot \tan(i)$$

$$K_{rc}(i) = \frac{K_{rc_0}}{\cos(i)}$$

where:

- K_{rc_0} is the initial radial cutting force coefficient.
- i is the inclination angle.

2.1.5 Regenerative Chatter, Stability Criterion, and Feedback Loops in Milling Operations

High-speed CNC milling faces significant challenges due to **regenerative chatter**, a self-excited vibration resulting from feedback between the cutting tool and the previously machined surface. This phenomenon directly affects machining stability, surface finish, and tool life by forming a feedback loop where the tool repeatedly encounters an uneven surface created during prior passes. Any slight deflection or vibration in the tool leaves a wavy surface on the workpiece, and subsequent tool passes re-engage with this surface, creating a regenerative effect. This feedback loop introduces a time delay T, governed by the spindle speed and tool engagement frequency. The current tool deflection $y(t)$ interacts with the delayed deflection $y(t-T)$, as represented in Figure 2.12.

$$h(s) = h_0(s) - (y(t) - y(t-T))$$

Where:

- $h_0(s)$ is the nominal chip thickness,

- $y(t)$ is the current tool deflection,
- $y(t-T)$ is the deflection from the previous pass.

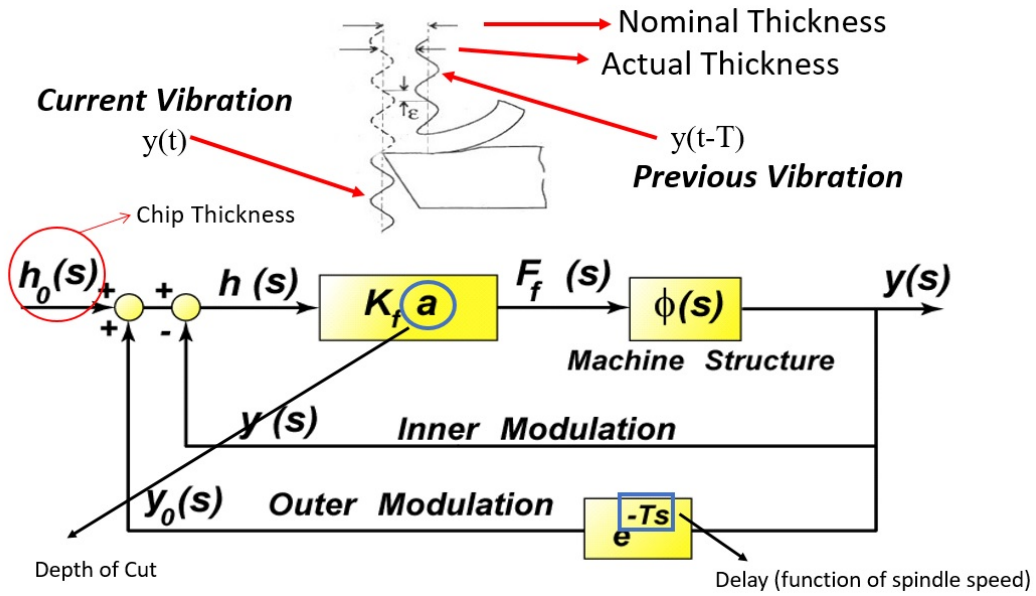

Figure 2.12: Control system representation of regenerative chatter in milling operations.

The **chip thickness** $h(s)$ is modulated by both the intended depth of cut and structural deflections in the machine. Variations in chip thickness lead to changes in the cutting force $F_f(s)$, which in turn amplify the tool's vibrations. This dynamic interaction between cutting forces and tool deflections forms a feedback loop that, if uncontrolled, causes unstable cutting conditions. In control system terms, the milling process acts as a closed-loop system where feedback delay from the spindle rotation repeatedly subjects the tool to vibrations from the previous pass, modeled by the time delay $-Ts$. If operating near the system's natural frequency, this feedback loop can cause an escalation in vibration amplitude, resulting in poor surface quality, reduced tool life, and possible damage to the machine tool.

To mitigate regenerative chatter, adjusting the spindle speed to disrupt this feedback loop can prevent the alignment of the tool's natural frequency with the tooth-passing frequency. **Stability lobe diagrams** are commonly used to map safe spindle speeds,

avoiding chatter-prone regions. Additionally, increasing machine damping or applying **adaptive control strategies** with real-time sensor feedback can stabilize cutting conditions by dynamically modifying cutting parameters.

Stability Criterion in Milling

Dynamic stability is essential for smooth, efficient milling and avoiding chatter onset. The stability of a milling operation can be analyzed via the system's **closed-loop transfer function**, which links tool displacement response y (representing the deflection or displacement of the cutting tool) to the nominal chip thickness h_0 (the intended depth of cut) based on applied cutting forces and machine structure.

$$\frac{y}{h_0} = \frac{K \cdot b \cdot \Phi(\omega)}{1 + K \cdot b \cdot \Phi(\omega) \cdot (1 - e^{-\tau i \omega})}$$

Where:

- y represents the tool's deflection or displacement,
- h_0 is the nominal or intended chip thickness,
- K represents system gain,
- b is the damping coefficient,
- $\Phi(\omega)$ is the frequency response function (FRF) of the machine structure,
- τ is the time delay from spindle rotation.

The system's stability limit is defined by the critical damping b_{lim} that satisfies the condition:

$$e^{-\tau i \omega} = -1$$

and can be expressed as:

$$b_{lim} = \frac{-1}{2K \cdot \min(\Re(\Phi(\omega)))}$$

When b exceeds b_{lim}, stability is maintained. Below this threshold, the system becomes unstable, leading to excessive vibrations and chatter.

Frequency Considerations for Stability

For practical stability, the ratio between the tool's natural frequency f_n and tooth-passing frequency f_t should ideally be an integer N, which keeps the forces and vibrations in phase and minimizes vibration amplification:

$$\frac{f_n}{f_t} = N$$

where N is an integer. The tooth-passing frequency f_t can be calculated as:

$$f_t(\text{turning}) = \frac{v_m[\text{RPM}]}{60}$$

$$f_t(\text{milling}) = \frac{v_m[\text{RPM}] \cdot z}{60}$$

where:

- v_m is the cutting speed in RPM,
- z is the number of tool teeth.

This approach ensures stable milling by aligning the tool frequency with cutting parameters, reducing the potential for chatter-induced instabilities.

2.1.6 Stability Regions and Instability

When the ratio f_n/f_t corresponds to an integer value (e.g., $N = 1$), the system achieves maximum stability. However, when this ratio deviates from an integer, instability begins to set in, leading to increased vibration amplitudes, as illustrated in the **stability**

lobe diagram. This diagram shows different regions of stability, with clear boundaries between stable and unstable cutting conditions.

For instance:

- At $N = 1$, the system is stable, with vibrations in phase and minimal amplitude.
- At $N = 1.25$, the system becomes unstable, as the frequency mismatch leads to forced vibrations, causing irregular surface finishes and potential tool damage.

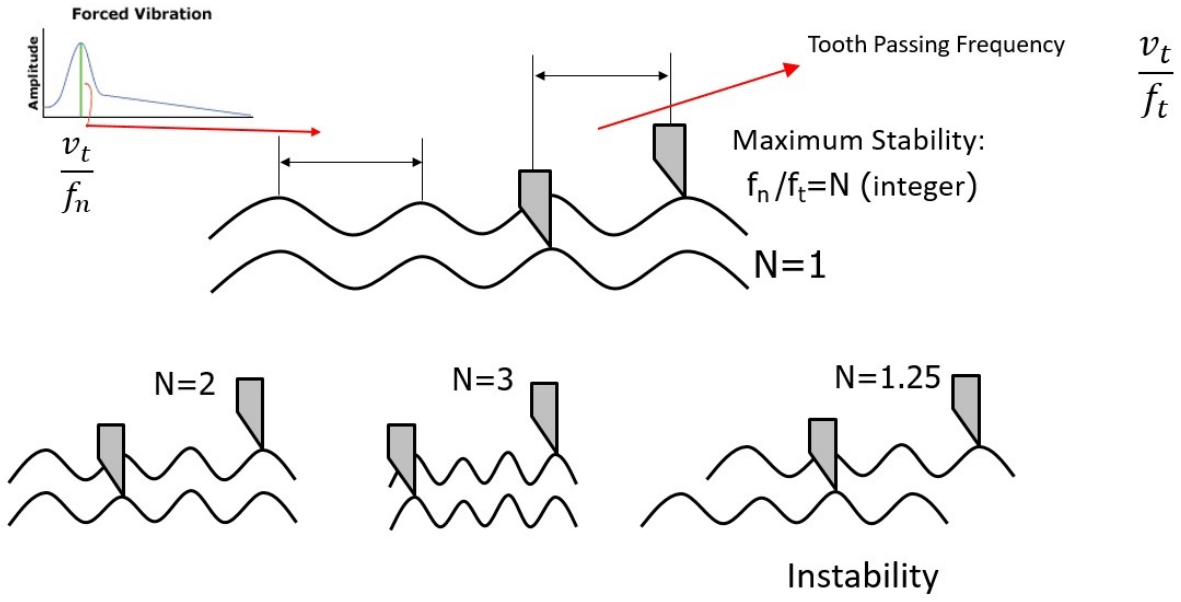

Figure 2.13: Stability and instability regions based on the ratio between the natural frequency f_n and the tooth-passing frequency f_t.

By carefully selecting the cutting speed and tool geometry, machinists can operate within the stable regions of the stability lobe diagram, avoiding the catastrophic effects of chatter.

2.1.7 Stability Lobe Diagram Analysis

The **stability lobe diagram** in Figure 2.14 provides a visual representation of stable and unstable regions in relation to the depth of cut and spindle speed. The highlighted lobes represent unstable regions where regenerative chatter is likely to occur. Conversely, the areas between the lobes represent stable regions where milling operations can be conducted without the risk of chatter.

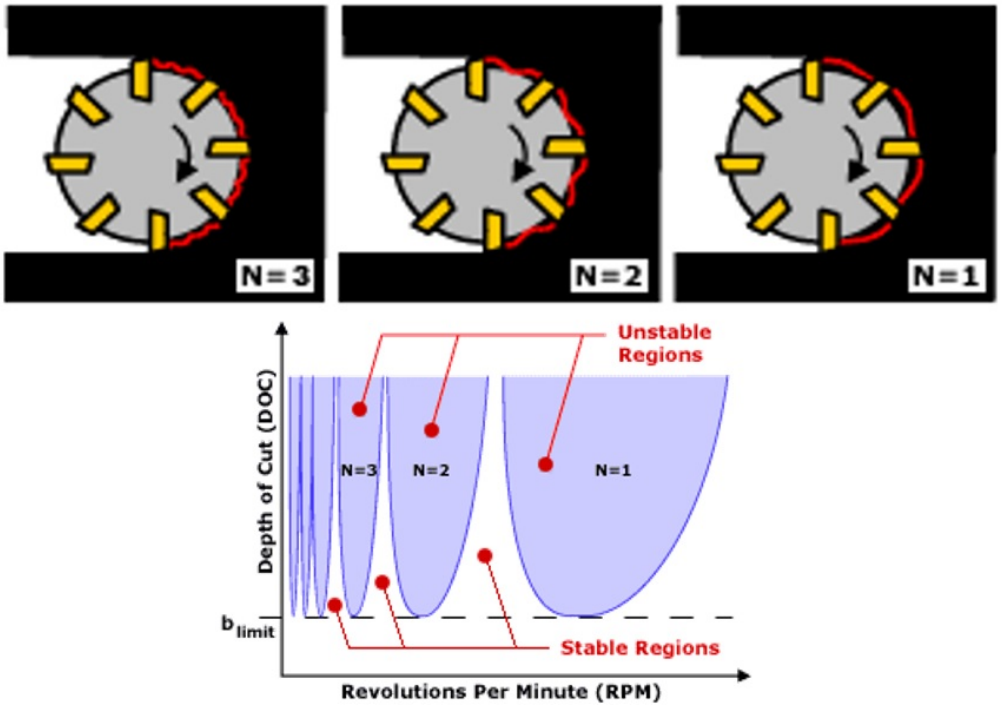

Figure 2.14: Stability lobe diagram showing the relationship between axial depth of cut and spindle speed.

In the diagram of lobes, we observe that for each ratio of f_n/f_t, multiple lobes appear, showing different stability zones. The situation repeats for every integer value of f_n/f_t, leading to these distinct lobes that help machinists optimize their spindle speed and depth of cut.

Analytical Calculation of the Stability Lobe Diagram

The analytical calculation of the stability lobe diagram can be visualized through the block diagram, which shows the interaction between the cutting forces $F_x = K \cdot b \cdot h(t)$ and the vibration of the tool $x(t)$ over time. As shown in Figure 2.15, the previous pass $x(t - \tau)$ influences the current pass, creating the regenerative effect that leads to the formation of lobes.

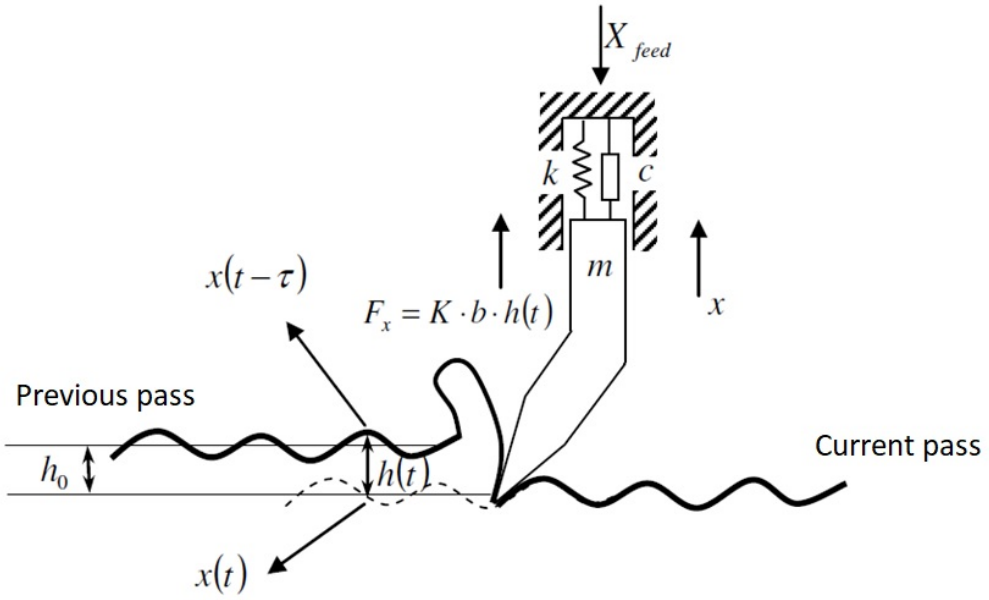

Figure 2.15: The interaction between cutting forces and tool vibrations.

In this model, the system's damping and stiffness (k, c) influence how the regenerative effect propagates through the machining process. Optimizing these parameters can help shift the system into stable regions of the stability lobe diagram.

2.1.8 Dynamic Cutting Forces in Milling

This section illustrates the relationship between dynamic displacements and cutting forces in the milling process.

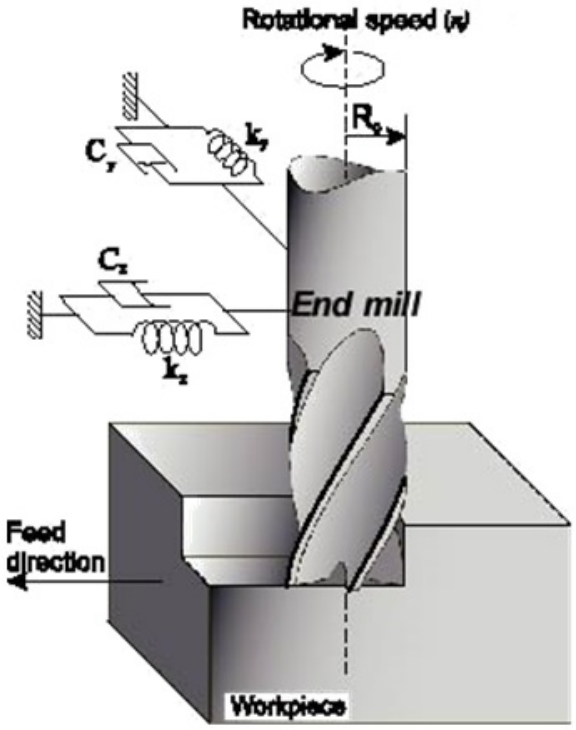

Figure 2.16: Schematic Representation of End Mill Cutter in Milling Operation

The cutting forces $\{\Delta F_x, \Delta F_y\}$ are represented as a function of dynamic displacements $\{\Delta x, \Delta y\}$, where the matrix $[A_0]$ describes the directional influence of these displacements on the forces. The function $f(\varphi_{st}, \varphi_{ex}, \frac{K_r}{K_t})$ incorporates the cutting angles and force coefficients, particularly considering the stiffness in the radial (K_r) and tangential (K_t) directions.

$$\begin{Bmatrix} \Delta F_x \\ \Delta F_y \end{Bmatrix} = \underbrace{\begin{bmatrix} A_0 \end{bmatrix}}_{f\left(\varphi_{st}, \varphi_{ex}, \frac{K_r}{K_t}\right)} \begin{Bmatrix} \Delta x \\ \Delta y \end{Bmatrix} \tag{2.1}$$

The cutting tool experiences vibrations influenced by both present and previous tooth impacts, denoted by $x(t-T), y(t-T)$, where T is the tooth passing period.

The primary factors affecting the cutting forces include:

- Cutting constants (material and tool geometry)
- Static chip thickness
- Vibrations during present and previous tooth periods
- Number of teeth (N)
- Immersion angle (φ_j)
- Axial depth of cut (a)

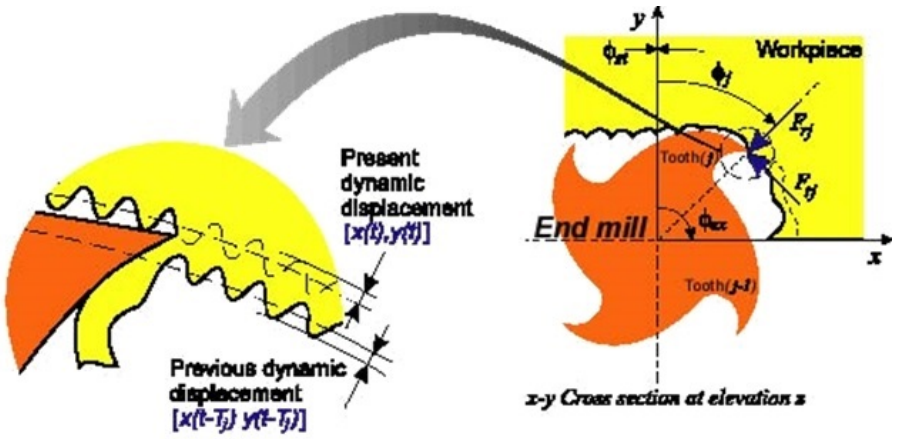

Figure 2.17: Influence of Present and Previous Dynamic Displacements in Milling Operations

2.2 Previous research on chatter and machine stability

Theories on Chatter in Milling

This section compares the theories related to chatter vibration in milling processes, divided into theories considering one degree of freedom (1 DoF) and two degrees of

freedom (2 DoF).

2.2.1 One Degree of Freedom Theories

Early research by Tlusty (1986)[13] contributed to the understanding of chatter by introducing analytical models that describe the vibration behavior in high-speed machining. Tlusty's work provided essential insights into the relationship between spindle speed, tool dynamics, and stability, particularly in the context of milling operations. Tlusty's model simplifies the vibratory motion in the milling plane to a single direction, averaged over the immersion angles of the tool. The stability analysis is reduced to a 1 DOF system, where the flexibility matrix is projected through directional factors.

Key Contributions by Tlusty

Tlusty made significant advancements in understanding and controlling chatter in machining processes, with his research particularly focusing on stability lobes and process damping as critical factors in mitigating chatter.

- **Stability Lobes**: Tlusty demonstrated that by selecting spindle speeds where the tooth passing frequency of the cutter aligns with the natural frequency of the machine structure, substantial improvements in machining stability can be achieved, even at high material removal rates. His research highlighted that stability lobes become increasingly important at high spindle speeds, where the regenerative chatter effect is more pronounced. Figure 2.18 visually demonstrates the regenerative chatter effect, which is central to Tlusty's work on stability. It shows how relative vibrations between the tool and workpiece lead to surface waviness, which regenerates into chatter during subsequent cuts.

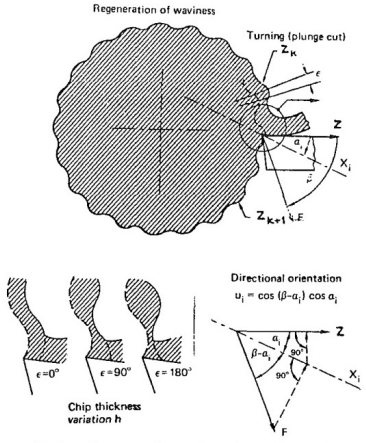

Figure 2.18: Regeneration of Waviness in Turning [Tlusty (1986)]

As spindle speed increases, the potential for greater stability arises in certain speed ranges, referred to as "lobes." Within these regions, even deeper cuts can be made without the onset of chatter. Tlusty's work involved deriving the limit of stability of chatter vibrations in both time and frequency domains, showing that at specific spindle speeds, there could be a considerable increase in stability, thus allowing higher cutting depths without inducing vibrations.

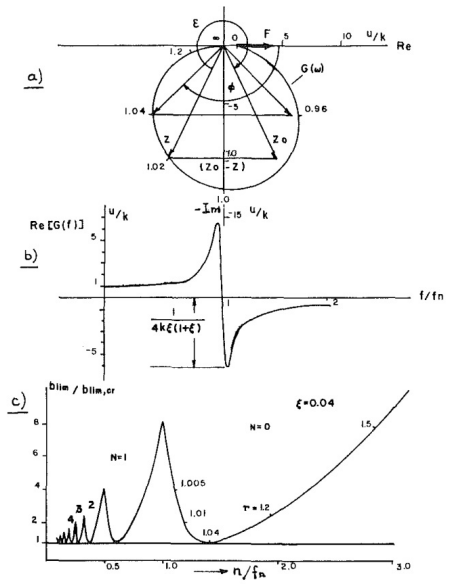

Figure 2.19: Deriving Stability Lobes[Tlusty (1986)]

Figure 2.19 graphically illustrates the process of deriving stability lobes, a key contribution of Tlusty's work. The stability lobes define operational boundaries where the system remains chatter-free.

- **Process Damping**: Tlusty also explored the role of damping in the cutting process, particularly at low spindle speeds. Process damping refers to the dissipation of vibrational energy through interaction between the cutting tool and the workpiece material. This damping effect stabilizes the cutting process by reducing the amplitude of vibrations, especially at low speeds. However, Tlusty noted that as spindle speed increases, the effect of process damping diminishes. He emphasized the importance of increasing the structural stiffness of the machine—especially the spindle and tool assembly—to maintain stability at higher cutting speeds, where process damping is no longer effective. His analysis showed that with advancements in spindle stiffness, achieved through design improvements such as larger diameter roller bearings, stability could be enhanced even during high-speed milling.

Tlusty's work provided a solid foundation for later developments in chatter prediction and control. His development of stability lobe diagrams (SLDs), a practical tool for predicting chatter-free operational conditions, remains a widely used method in modern machining dynamics, particularly for high-speed milling operations. By analyzing the interaction between spindle speed, cutting force, and machine dynamics, Tlusty's research offered practical guidelines for selecting spindle speeds and cutting parameters to mitigate the risk of chatter, thereby improving machining efficiency and surface quality.

2.2.2 Two Degrees of Freedom Theories

The study by Altintas and Budak (1995)[14] introduces a novel analytical method for predicting stability lobes in milling processes, which are critical for determining chatter-free conditions. The method relies on the dynamic properties of the machine tool-workpiece system and approximates the time-varying cutting force coefficients using a Fourier series expansion. This approach allows for the calculation of spindle speeds and axial depths

of cut without the need for iterative numerical solutions, distinguishing it from previous methods. In fact Altintas proposed a "**zero-order approach**" using a Multiple Input Multiple Output (MIMO) system with 2 DoF, allowing for vibrations in multiple directions. This model assumes that the average cutting force closely approximates the instantaneous force when multiple cutting edges are engaged simultaneously.

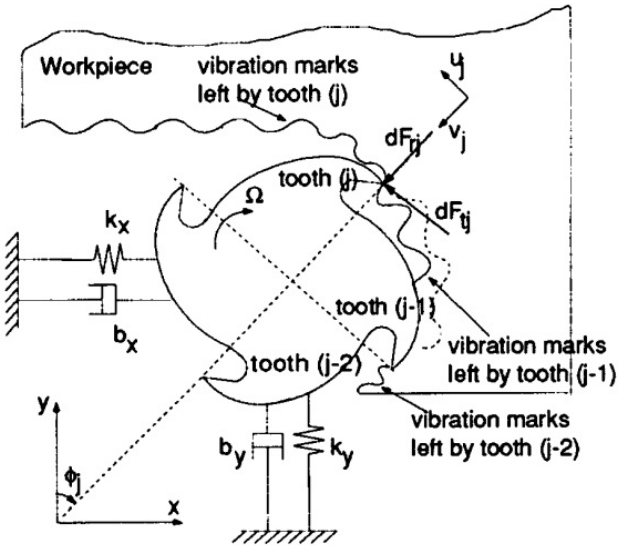

Figure 2.20: Dynamic model of milling with two degrees of freedom [Altintas and Budak]

Moreover, Recent research by Celikag, Ozturk, and Sims (2021) [16] explored the possibility of mode coupling chatter in milling, a self-excited vibration phenomenon traditionally associated with processes like threading. The authors specifically examined whether mode coupling chatter can occur in robotic milling operations and compared it with regenerative chatter—the more established mechanism in milling.

Key Contributions by Altintas and Budak

- **Analytical Stability Prediction**: Altintas and Budak introduced a novel closed-form solution for stability lobe prediction in milling. By approximating time-varying cutting force coefficients with Fourier series, their method directly com-

putes critical spindle speeds and axial depths of cut, bypassing the need for time-domain simulations and iterative methods that were standard in previous models by Tlusty and Tobias.

- **Dynamic Milling Force Model**: Their model incorporates dynamic milling forces by accounting for the time-varying nature of cutting forces, which are influenced by tool vibrations. This approach enables the accurate representation of total chip thickness and cutting forces during milling, providing an enhanced prediction of stability under varying machining conditions.

- **Characteristic Stability Equation**: A significant contribution was the derivation of a characteristic equation based on the transfer functions of the machine tool structure and the Fourier-expanded cutting force coefficients. This equation allows for the analytical determination of stable cutting conditions, facilitating the prediction of chatter-free spindle speeds and depths of cut for a given chatter frequency.

- **Validation with Experimental Data**: Altintas and Budak validated their method against both time-domain simulations and experimental data, showing strong agreement with earlier experimental results (e.g., Opitz, 1968) and numerical methods (e.g., Smith and Tlusty, 1990). This validation underscored the practical applicability of their model.

- **CAD/CAM Integration Potential**: Their analytical model has practical implications for CNC machining, enabling real-time process planning. This model, which can be integrated into CAD/CAM systems, provides a fast and accurate method for predicting stable cutting conditions, optimizing tool paths, and reducing machining vibrations.

- **Advancement Over Prior Models**: The approach by Altintas and Budak represents a substantial improvement over previous stability models, especially those focusing on simpler orthogonal cutting operations. Their method is more suited to

milling's complexities, where cutting forces vary dynamically and system dynamics are more intricate.

Key Insights from Celikag & Ozturk on Mode Coupling Chatter in Milling

- **Rejection of Mode Coupling Chatter in Milling**: Celikag and Ozturk demonstrated, both theoretically and experimentally, that mode coupling chatter is not applicable in milling. Unlike threading, where cutting occurs on a new surface with each pass, milling involves cutting over a previously machined surface, resulting in a regenerative mechanism rather than mode coupling chatter.
  Figure 2.21 illustrates the coupled chatter system in threading operations, highlighting the absence of regeneration, contrasting with the regenerative chatter mechanism typical in milling.

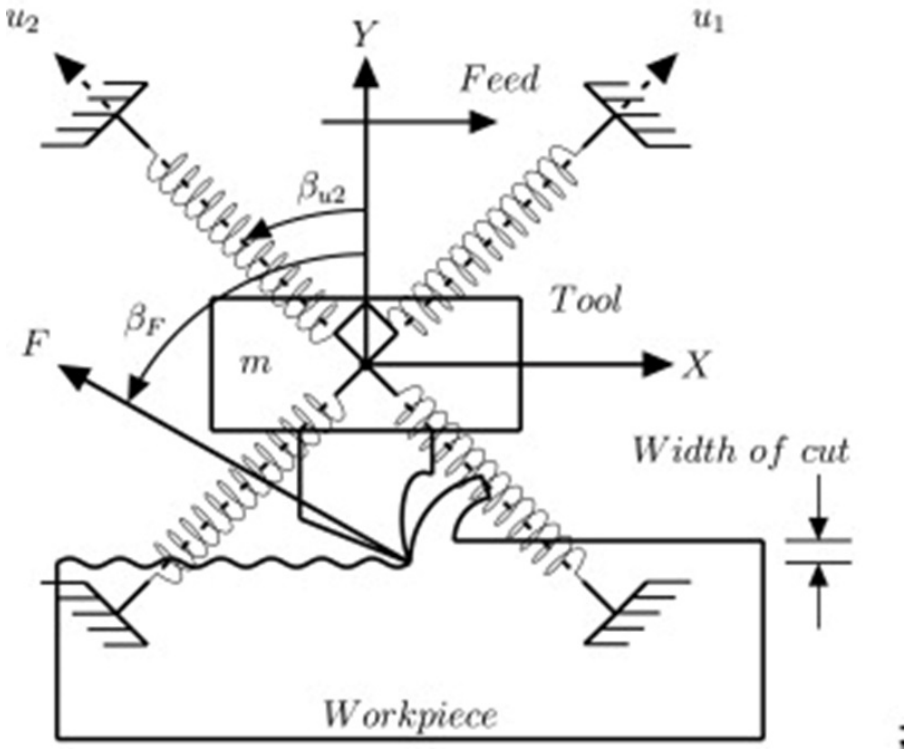

Figure 2.21: Theoretical model of asymmetrical boring bar of a coupled system [Celikag, Ozturk, and Sims].

- **Experimental Validation**: The authors validated their findings through robotic milling experiments, showing that stability boundaries predicted by mode coupling chatter models were inconsistent with experimental results. Their research further confirmed that regenerative chatter dominates milling, as the process stability is highly dependent on spindle speed, a factor unaccounted for by mode coupling chatter predictions.

- **Practical Implications**: This study clarifies previous ambiguities in the literature by demonstrating that mode coupling chatter is not a concern in milling. It emphasizes the necessity of modeling stability boundaries based on regenerative chatter mechanisms for accurate predictive results.

2.2.3 Critical Analysis of Research Gaps

Research Gaps in Chatter Prediction

Despite advances in chatter prediction, challenges persist, especially in accurately modeling damping at the spindle-holder-tool interface. Variability in tool wear, clamping force, and surface irregularities introduce uncertainties, impacting high-speed milling. Current models often approximate these nonlinear interactions, limiting predictive reliability. Thermal effects also remain underrepresented; heat generated in high-speed cutting alters material properties, affecting stiffness and damping and exacerbating vibrations. As temperatures rise, components expand, shifting stability regions—an issue rarely integrated into traditional models. Additionally, adaptive machining environments add complexity, with real-time variable cutting speeds and material properties that traditional models struggle to accommodate. Machine learning offers a promising solution, leveraging data to predict chatter onset and adjust parameters dynamically. Addressing these gaps calls for enhanced modeling of spindle-holder interactions, thermal effects, and adaptive chatter control via data-driven methods.

Research Gaps in Finite Element Modeling (FEM)

While FEM is critical in dynamic CNC analysis, gaps remain in modeling damping mechanisms at interfaces like the spindle-tool-holder. Real-world damping is nonlinear and affected by cutting forces, temperature, and wear, but FEM models typically simplify these factors. Studies by Ringgaard et al. (2019)[17] show improved FEM predictions through interface modeling, but precise damping effects are challenging to capture. Thermal effects, often decoupled from dynamics in FEM, are also crucial; as Altintas et al. (2008)[18] indicate, temperature-induced changes in stiffness and frequency affect stability in high-speed milling, yet models frequently overlook this. Tool deflections and transient behaviors under varying conditions are additional gaps. While semi-discretization methods by Altintas et al. improve stability predictions, computational demands limit industrial feasibility. Overcoming these gaps requires advanced nonlinear damping models, thermo-mechanical integration, and enhanced real-time response methods for FEM's reliability in high-speed, precision operations.

Research Gaps in Stability Lobe Diagrams

Stability Lobe Diagrams (SLDs) remain essential but lack accurate modeling of joint dynamics, especially at the spindle-holder-tool connection. Joint dynamics depend on clamping force, surface roughness, and thermal effects, all affecting stability limits. Current models often simplify these variables, leading to prediction inaccuracies. Tool wear further complicates SLDs, as it alters system stiffness and damping, shifting stability zones. While machine learning could enable real-time SLD adaptation to changing conditions like tool wear, thermal expansion, or material variability, implementation challenges remain, including robust sensor networks and processing capabilities. Advancements in joint dynamic modeling, wear integration, and ML-enhanced stability predictions will be crucial for optimizing productivity, surface quality, and tool life in CNC machining.

Chapter 3

Methodology

3.1 Description of the Dynamill G5 Gantry Milling Machine

The **Dynamill G5** is a high-performance, gantry-type 5-axis machining center designed to achieve precision and efficiency. Its rigid gantry structure ensures excellent stability and makes it ideal for high-speed machining operations.

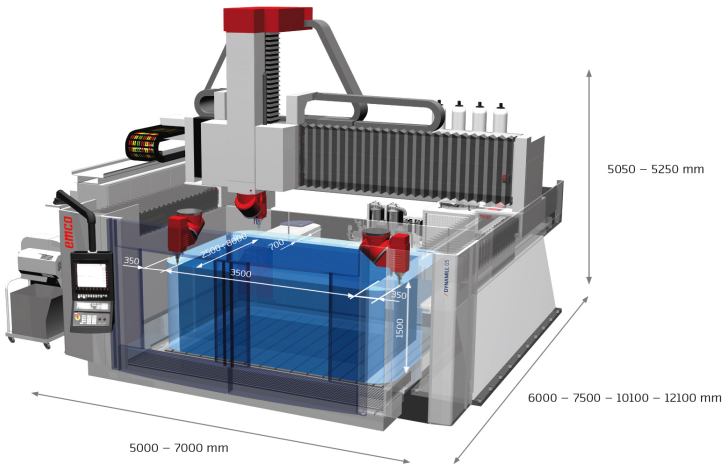

Figure 3.1: Overall dimensions & Working Envelope of the Gantry Milling Machine Dynamill G5

Structural Features

- **Gantry Design**: Provides exceptional rigidity and dynamic stability, ensuring precise machining.
- **Axis Configuration**:
  - **X-axis**: Travel range from 2500 mm to 8000 mm.
  - **Y-axis**: Up to 3500 mm.
  - **Z-axis**: Configurable to 1300 mm or 1500 mm.
  - **Feedrate**: Capable of up to 40 m/min with an acceleration of 4 m/s^2.
- **Integrated Z-Axis Saddle**: Enhances stiffness and machining accuracy.

Milling Head and Spindle

- **Direct-Drive Milling Heads**: Offer high dynamics and precision.
- **Spindle Speeds**: Up to 24,000 rpm with power configurations reaching 74 kW and 615 Nm torque.
- **Undercut Capability**: 15° or 20° for improved accessibility in complex geometries.

Additional Features

- **Tool Changer**: Supports up to 200 tools for automation.
- **Control Systems**: Incorporates advanced CNC systems such as Heidenhain TNC 640 HSCI or Sinumerik ONE.

3.2 Simulation Tools and Techniques

The dynamic behavior of the Dynamill G5 is analyzed using Finite Element Method (FEM) modeling in CATIA V5 software. The FEM analysis is conducted in two main phases: static analysis and modal analysis. The model incorporates critical structural and dynamic characteristics, such as mass, stiffness, and damping properties, to simulate the machine's behavior accurately.

3.2.1 Static Analysis

In the static analysis, a force of 10,000 N is applied to the considered points in the X and Y directions of the machine. Displacements are measured, and stiffness values are computed based on the system's response. Connections within the machine structure, such as those made with profiled rails, sliding blocks, gear reducers, and ball screws, are modeled using concentrated stiffness values provided by manufacturers (e.g., BOSCH). Bolted and screwed elements are assumed to have infinite stiffness, while connections between the ram and the spindle nose are modeled as a virtual, infinitely rigid part, based on known displacement values from experimental tests.

The stiffness properties of key connection systems, such as the rack-and-pinion mechanism, upper support, and lower support, are modeled with specific translational and rotational stiffness values, as shown in Figure 3.2. For instance:

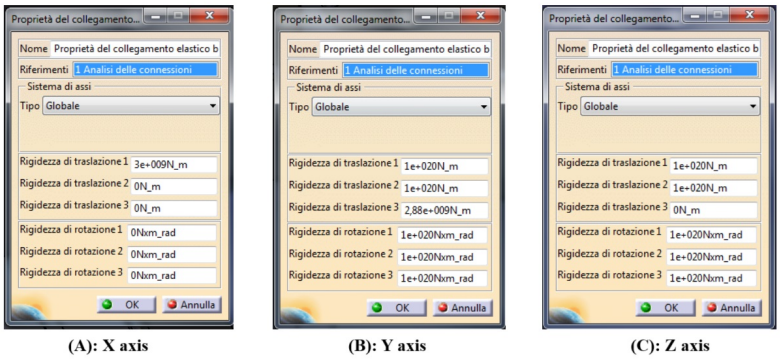

Figure 3.2: Stiffness properties of (A) the rack-and-pinion connection, (B) upper support, and (C) lower support.

- The **rack-and-pinion connection** is modeled with a high translational stiffness of 3×10^9 N/m in one direction and zero stiffness in other degrees of freedom.
- The **upper support connection** assumes near-infinite translational stiffness (1×10^{20} N/m) in most directions, with a specific direction set to 2.88×10^9 N/m. Rotational stiffness values are also set to 1×10^{20} Nm/rad.
- The **lower support connection** exhibits infinite translational stiffness in two directions and zero stiffness in the third direction. Rotational stiffness values are again modeled as near-infinite.

To validate the static model in CATIA, experimental results have been obtained. In the static tests, various force values are applied near the nose of the spindle, and deformations are measured using a dial indicator. This approach allows for the calculation of the static stiffness of the machine and the evaluation of linear behavior in the system's response. These experimental results are compared with the simulation outcomes in CATIA to ensure the accuracy and reliability of the static model.

3.2.2 Modal Analysis

The modal analysis is performed by solving the eigenvalue problem:

$$-\omega^2[M]\{f\} + [K]\{f\} = 0 \quad \rightarrow \quad \omega_i = \sqrt{\frac{k_i}{m_i}}$$

using the same geometry, materials, constraints, and discretization from the static analysis. The stiffness matrix is identical to that of the static model. The model considers the weights of key structural components, including the supports, the spindle motor (applied at its center of gravity), and the head and axis C platform. Masses distant from the tool point, such as pedestals or cabinets, are excluded. The first 38 vibration modes are identified, providing insights into the machine's dynamic behavior.

3.3 Experimental Setup and Procedures

Experimental modal analysis (EMA) is conducted to validate the FEM model predictions and further analyze the machine's dynamic performance. The experimental setup includes the following equipment provided by Dewesoft:

- **Dewesoft IOLITE® 8xACC IEPE/ICP Amplifier**: An 8-channel vibration measurement module designed for modal testing and structural dynamics analysis.
- **PCB 086C04 Impact Hammer**: Used to apply excitation forces for modal testing (specifications in the Appendix).
- **PCB 356A45 Triaxial Shock Accelerometer**: Measures the system's response to excitation forces (specifications in the Appendix).
- **Dewesoft-X-PROF Software**: Facilitates data acquisition and modal analysis.

3.3.1 Experimental Procedure

The Experimental Modal Analysis (EMA) was performed using a hammer with a **rubber tip** (Figure 3.3). The rubber tip was selected for its *low stiffness*, which helped to reduce the occurrence of double-hits and ensure more accurate force signals. This is particularly important in modal testing, as double-hits can distort the force signal and lead to unreliable Frequency Response Function (FRF) measurements. Furthermore, the rubber tip's damping properties helped to ensure that the excitation energy was more concentrated in the relevant frequency range, avoiding the broader spectral excitation produced by harder tips. As a result, the rubber tip enabled a more precise measurement of the machine's dynamic compliance and the extraction of FRFs without significant high-frequency noise.

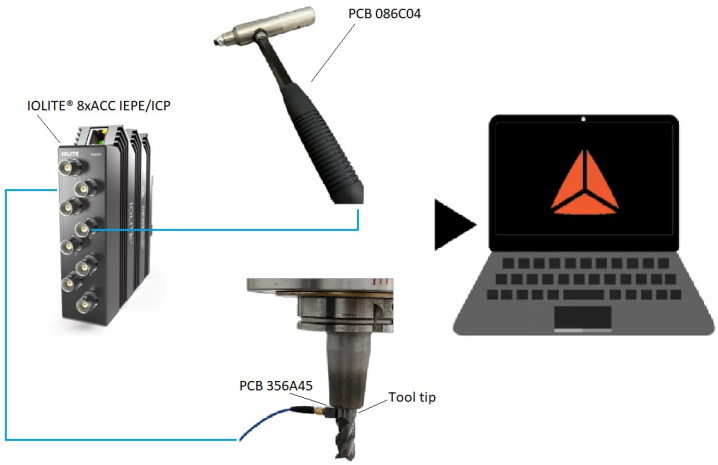

Figure 3.3: Experimental Modal Analysis Setup Schematic

The data acquired using Dewesoft-X-PROF software included the following:

- Frequency Response Functions (FRFs) and coherence graphs
- Damping estimation via the modal circle fit method
- Mode Indicator Function (MIF) for mode shape identification

This data was subsequently analyzed to correlate the damping estimates with the mode shapes, by identifying the frequency peaks observed in the MIF graph.

These experimentally derived FRFs were subsequently input into MillingStab software to generate stability lobe diagrams. The results were compared with simulation outputs to ensure accuracy and reliability.

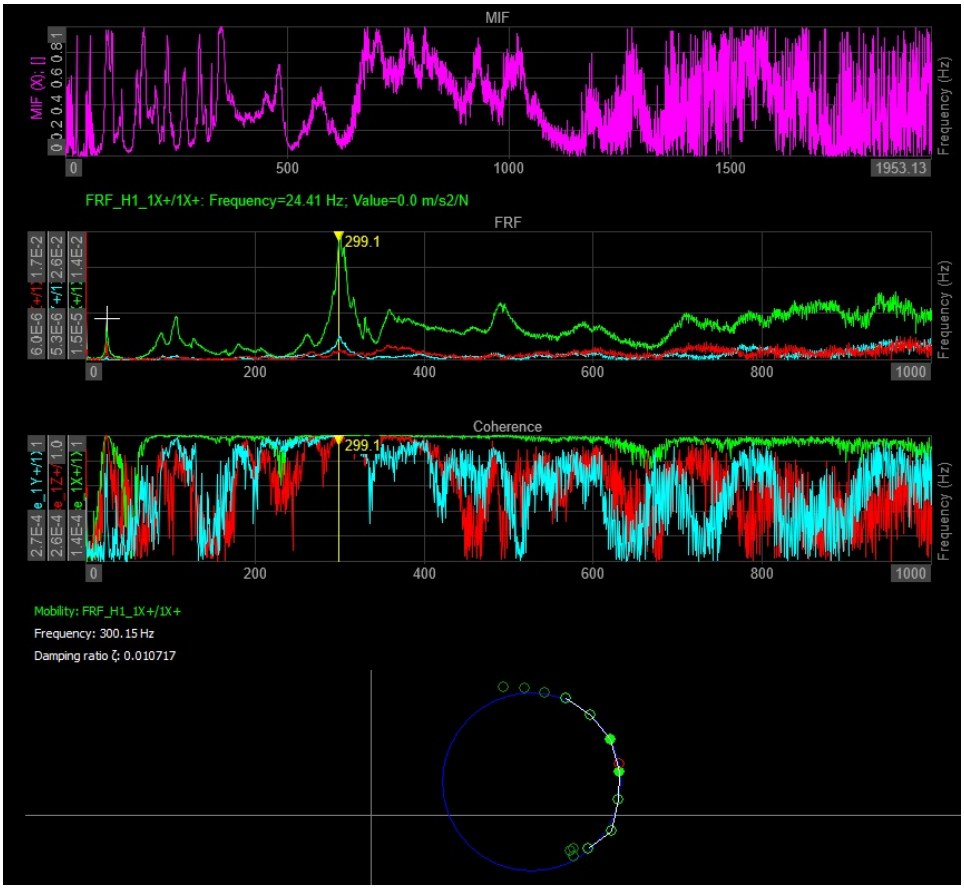

Figure 3.4: Analysis of MIF, FRFs, Coherence, and Modal Circles in Dewesoft-X-PROF

3.4 Stability Lobe Diagram Computation Using MillingStab Software

The Frequency Response Functions (FRFs) are determined at key points from both simulation and experimental results to assess vibrational behavior under different operational conditions. These FRFs are then used to generate stability lobe diagrams through MillingStab software, developed by CNR STIIMA. The stability lobe diagrams provide a comprehensive understanding of the machine's operational stability, highlighting combinations of spindle speed and depth of cut that avoid chatter and ensure efficient machining performance.

3.4.1 Initial Setup and Input Parameters

The process begins with defining machining parameters in the Process Definition Section (Figure 3.5), Key inputs include:

- **Number of Flutes**: Defines the tool's cutting edges.
- **Shear Coefficients** (K_r, K_t): Represent material cutting resistance.
- **Engagement Angles**: Specify tool entry and exit points in the workpiece.
- **Spindle Rotation Direction**: Impacts chip evacuation and cutting dynamics.

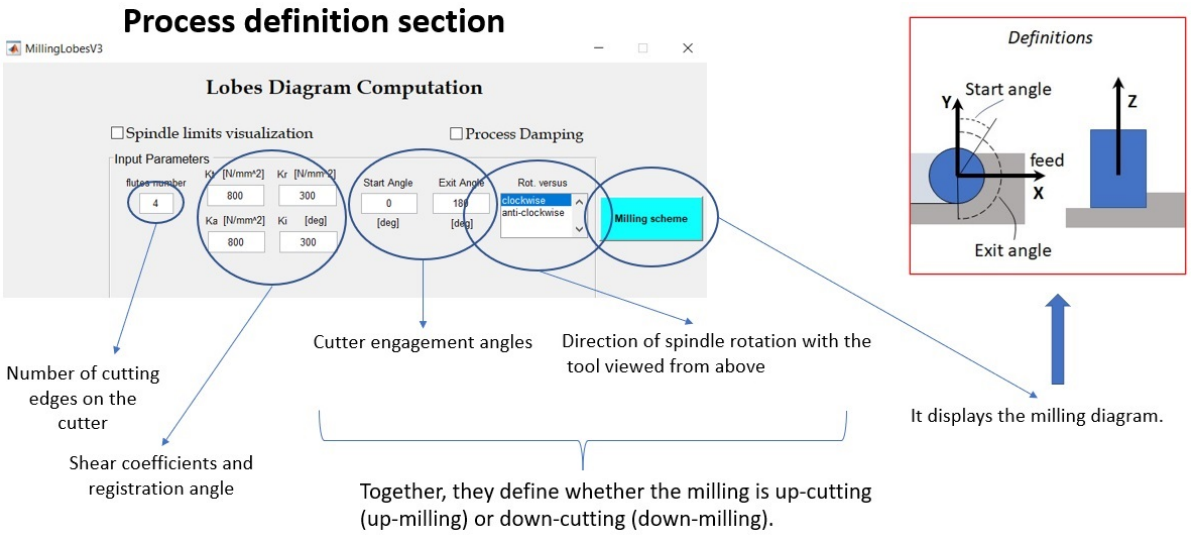

Figure 3.5: Detailed View of the Process Definition Section

3.4.2 FRF Insertion and Stability Analysis

FRFs are loaded into the software for each directional mode (FRF_{XX}, FRF_{YY}, etc.). The selected frequency range ensures focus on the operational bandwidth. After defining parameters, the system computes stability lobes, displaying spindle speed and depth of cut combinations for stable operation (Figure 3.6).

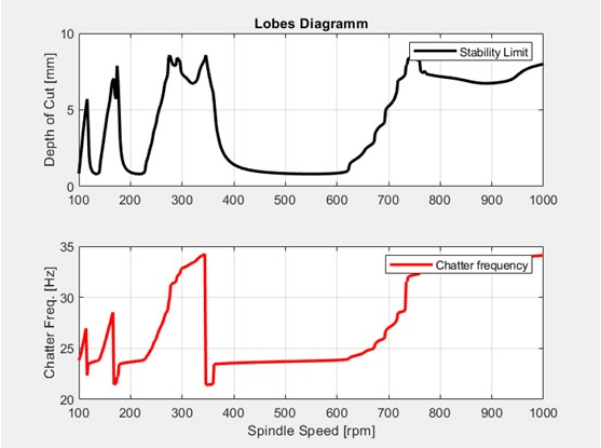

Figure 3.6: Stability Lobes Diagram Calculation

Chapter 4

Results and Discussion

This chapter analyzes the **dynamic behavior of CNC machine tools** using both *experimental modal analysis (EMA)* and *finite element modeling (FEM)*. The results focus on the machine's structural responses, stability, and damping characteristics, providing insights for accurate chatter prediction and machining process optimization.

The chapter includes:

1. **Mode Shapes and Natural Frequencies:** Identification of modal frequencies and their discrepancies between EMA and FEM, emphasizing damping effects.

2. **Frequency Response Functions (FRFs):** Examination of EMA and FEM results, comparing resonance frequencies, dynamic compliance, and coherence to assess structural behavior and model accuracy.

3. **Stability Lobe Diagrams:** Analysis of stability limits using various FRF configurations, with comparisons between EMA and FEM-based diagrams to understand milling process dynamics.

This chapter combines experimental and numerical findings to explore key factors affecting CNC machine stability and performance.

4.1 EMA Results

The DewesoftX software was successfully configured, and the designated points shown in figure 4.1 were excited using the instrumented hammer. Each point was struck multiple times to ensure data reliability and minimize errors.

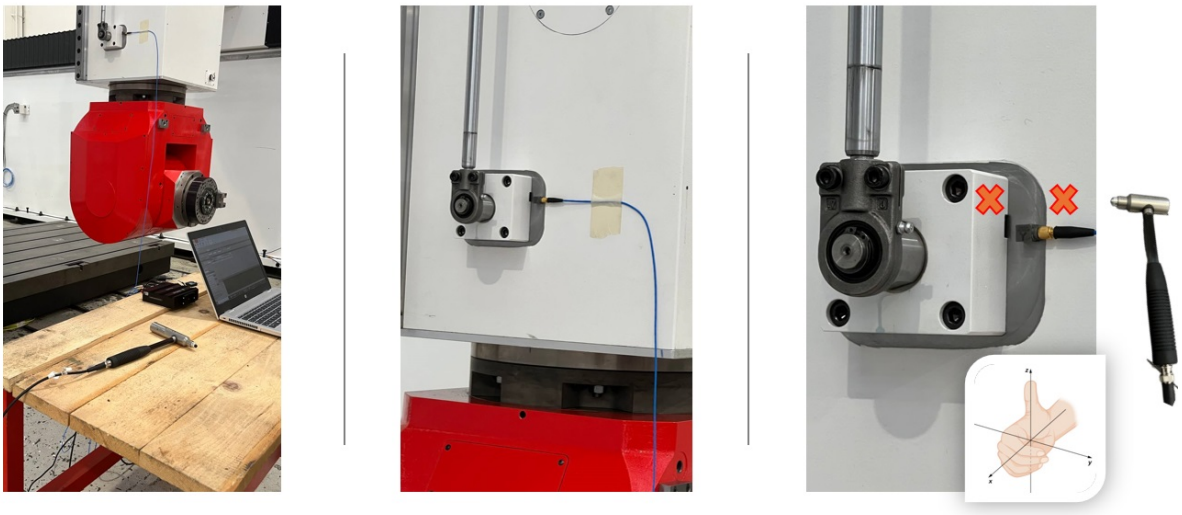

Figure 4.1: The setup for data acquisition.

Figures 4.2 and 4.3 provide a detailed analysis of the frequency response of the machine tool subjected to force in the X and Y directions, respectively.
The analysis includes the time-domain response, magnitude and phase of the Frequency Response Function (FRF), and the coherence function for the X, Y, and Z directions.

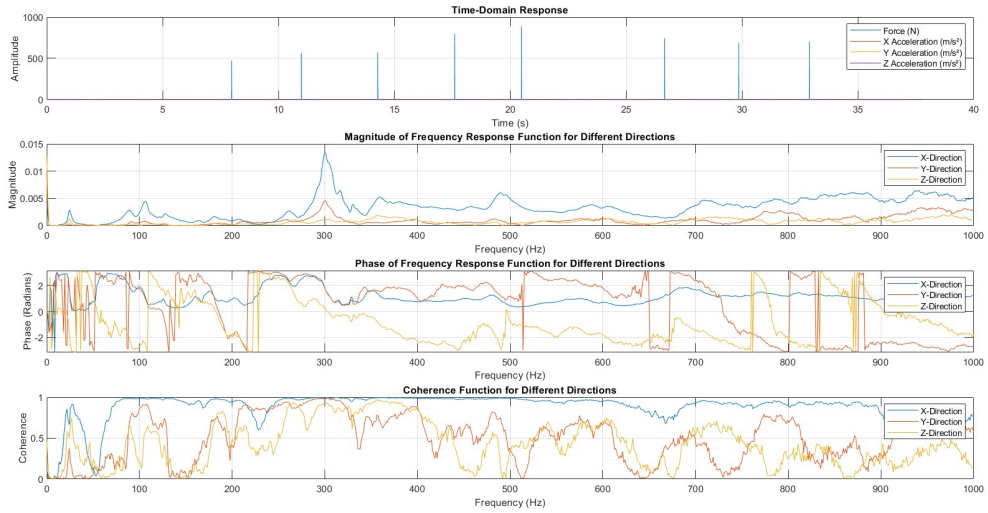

Figure 4.2: Frequency Response Analysis of the Machine Tool with force applied in X direction.

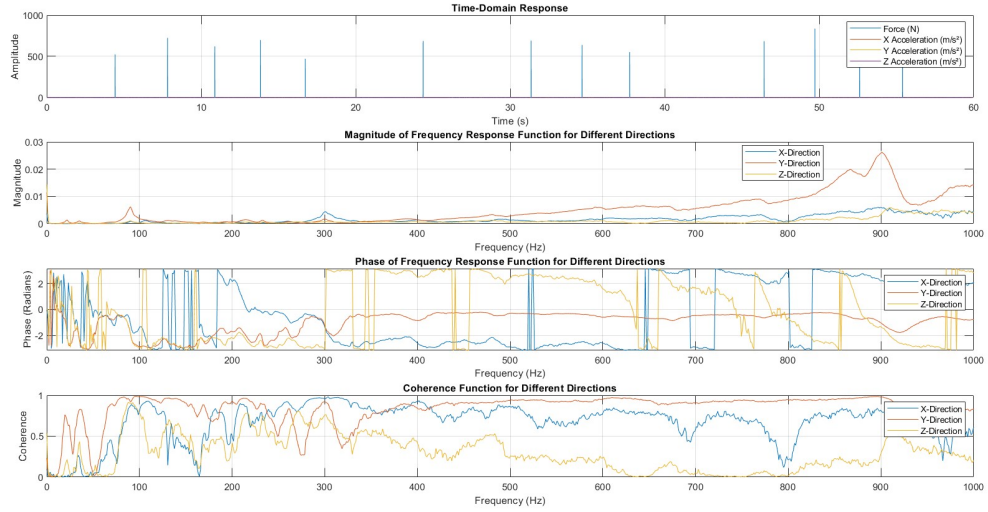

Figure 4.3: Frequency Response Analysis of the Machine Tool with force applied in Y direction.

Analyzing the figures reveals notable discrepancies in the coherence functions between the X and Y directional excitations.

Under excitation in the **X direction**, the coherence values indicate reliable measurements and a strong input-output correlation, despite some declines at certain frequencies, likely attributed to noise or limitations in the measurement setup. In contrast, for **Y-direction excitation**, comparing to X direction, lower coherence values are observed across the frequency spectrum. This behavior suggests that the machine structure exhibits greater stiffness in the Y direction, limiting the energy transfer during impact testing. Attempts to increase the impact force by applying harder impacts resulted in wear on the rubber and hammer tip, yielding minimal improvement. Consequently, in some calculations, only experiments with force applied in the X direction are analyzed due to the higher coherence values and stronger input-output correlation observed in this direction. This focused approach ensures more accurate chatter prediction and prevention, ultimately contributing to improved performance and stability in CNC machine tool operations.

Another significant observation is the diminished coherence below 10 Hz in both X and Y directions, accompanied by an upward drift in FRFs, indicating reduced data reliability. This limitation is commonly observed in systems utilizing piezoelectric accelerometers, which often struggle to capture low-frequency dynamics. Addressing these challenges may require employing a heavier impact hammer, a softer hammer tip, and more sensitive accelerometers.

4.2 Mode Identification Analysis

4.2.1 EMA Analysis

A detailed analysis of peak characteristics, including sharpness, phase shift, and damping behavior, is essential for mode identification. As previously mentioned, the results in the Y direction exhibited lower coherence values and unreliable outputs; therefore, this section focuses solely on experiments with force applied in the X direction.
In this context, the EMA results provided a summarized Mode Indicator Function (MIF) graph for the entire dataset. Analyzing the MIF graph revealed numerous resonance

peaks, distributed in clusters across the examined frequency range.

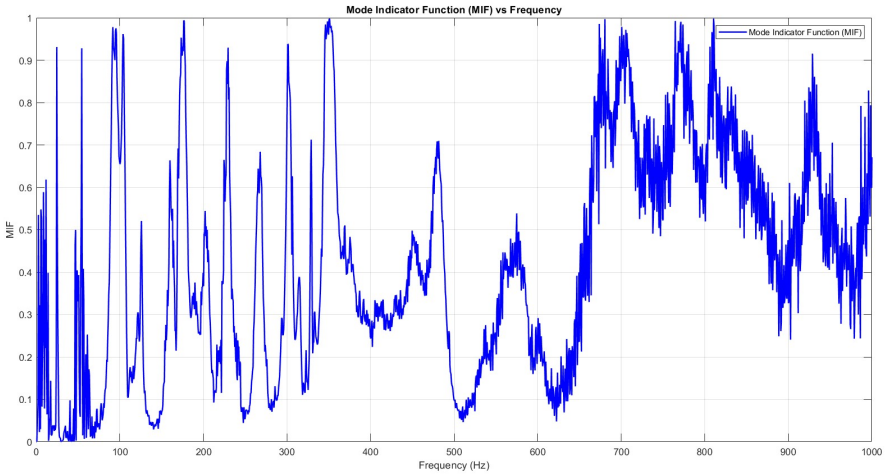

Figure 4.4: MIF (Mode Indicator Function) plot

It is essential to recognize that not all peaks observed in the FRF represent true mode shapes. Only those corresponding to the system's natural frequencies, where significant resonance leads to an amplified dynamic response, are identified as genuine modal peaks.

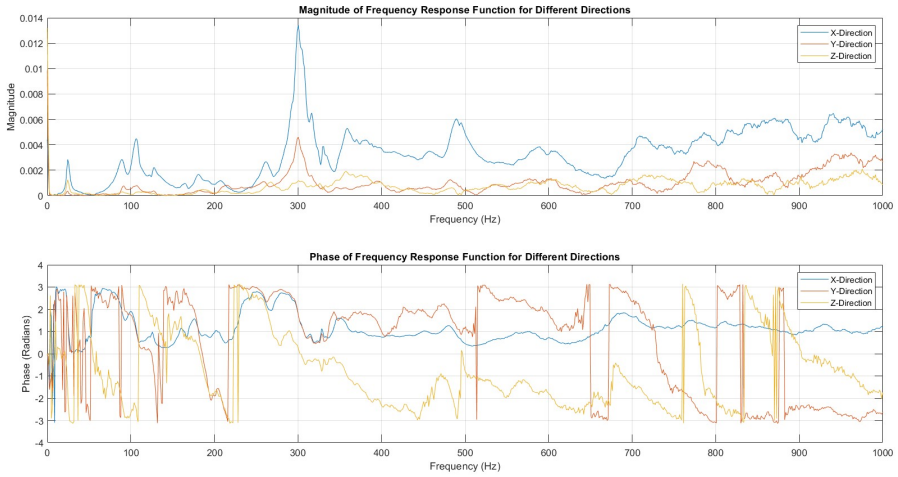

Figure 4.5: Magnitude and Phase plot of FRF for Different Directions

Based on the previous criteria, two distinct modes were identified at frequencies of

24.3 Hz and **300.1 Hz**, with corresponding damping ratios of $\zeta = 0.02$ and $\zeta = 0.01$, respectively. These modes were characterized and confirmed based on the sharpness of the resonance peaks, phase behavior, and damping characteristics as observed in the Frequency Response Function (FRF) and Mode Indicator Function (MIF) graphs.

Mode at 24.3 Hz ($\zeta = 0.02$)

The mode at 24.3 Hz exhibits a moderately sharp resonance, characteristic of a damped dynamic response. The broader resonance peak in the Frequency Response Function (FRF) indicates significant energy dissipation, aligning with the damping ratio ($\zeta = 0.02$). A rapid 180° phase transition around this frequency confirms resonance behavior, with the real part of the FRF crossing zero and the imaginary part peaking, signifying maximum energy exchange. The Nyquist plot shows a diffused trajectory, consistent with a moderately damped system.

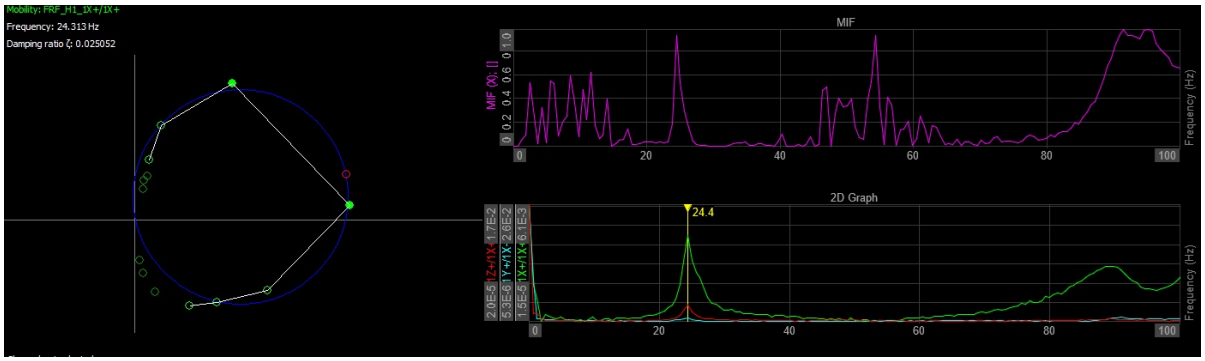

Figure 4.6: Mode shape visualization at 24.3 Hz generated in DewesoftX software.

Mode at 300.1 Hz ($\zeta = 0.01$)

At 300.1 Hz, the mode is sharply defined, reflecting a highly resonant behavior with minimal energy dissipation. The narrow peak in the FRF, coupled with a lower damping ratio ($\zeta = 0.01$), indicates strong amplification. A rapid 180° phase change around this frequency, along with the real part crossing zero and the imaginary part peaking, verifies resonance. The Nyquist plot confirms this observation, revealing a tightly clustered

trajectory indicative of a lightly damped system.

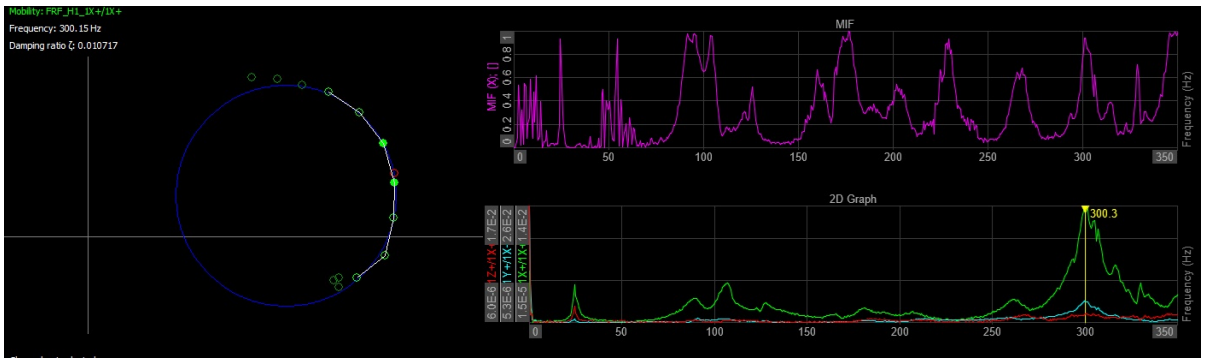

Figure 4.7: Mode shape visualization at 300.1 Hz generated in DewesoftX software.

General Observations

The analyses confirm the presence of natural frequencies at 24.3 Hz and 300.1 Hz, validated by the FRF, phase, and Nyquist plots. The sharper resonance and lower damping at 300.1 Hz highlight its stronger dynamic response compared to the moderately damped mode at 24.3 Hz. Both modes were derived from X-direction excitation, which provided higher coherence and reliability compared to the Y-direction.

4.2.2 FEM Analysis

FEM analysis provided a more significant number of modes compared to those identified by EMA. It is reasonable to assume that the lower number of modes obtained from the experimental test is due to the restriction of data collection to the z-axis. The FEM analysis gives a series of modes at the following frequencies:

Table 4.1: Modal frequencies obtained from FEM

Mode	Frequency (Hz)	Mode	Frequency (Hz)
1	13.713	20	112.491
2	14.289	21	115.495
3	14.662	22	117.745
4	17.835	23	122.531
5	19.488	24	124.611
6	22.519	25	132.279
7	35.036	26	132.311
8	39.017	27	134.634
9	44.846	28	135.848
10	64.841	29	141.176
11	69.016	30	143.716
12	71.577	31	150.626
13	73.095	32	163.773
14	74.033	33	172.897
15	82.944	34	178.191
16	83.757	35	179.918
17	102.602	36	182.415
18	108.476	37	185.421
19	109.971	38	193.668

The first three to four modes are not particularly important in the context of milling stability. These low-frequency modes typically represent rigid-body motions or global structural deformations, which have minimal influence on the dynamic behavior of the machine tool during normal operation. Such modes are generally constrained or heavily damped under standard machining conditions.

The frequencies listed in Table 4.1 represent the natural frequencies of the system, as calculated by the finite element method (FEM) software. These frequencies correspond to the inherent vibrational characteristics of the structure, encompassing both global and

local vibration modes. Higher-frequency modes are more critical for evaluating dynamic compliance and stability in machining operations, while the lower modes primarily offer insight into the broader dynamic range of the system.

4.2.3 Comparison of EMA and FEM Analyses

Correlation Metric Analysis

To assess the alignment between the dynamic responses obtained from the Experimental Modal Analysis (EMA) and the Finite Element Model (FEM), a correlation metric was introduced. This metric, while not equivalent to the Modal Assurance Criterion (MAC) due to the absence of full mode shapes, serves as a practical indicator of similarity. It compares the normalized Frequency Response Function (FRF) magnitudes at a single output position. The heatmap in Figure 4.8 visually represents the computed correlation metric, highlighting the relationship between the respective modes.

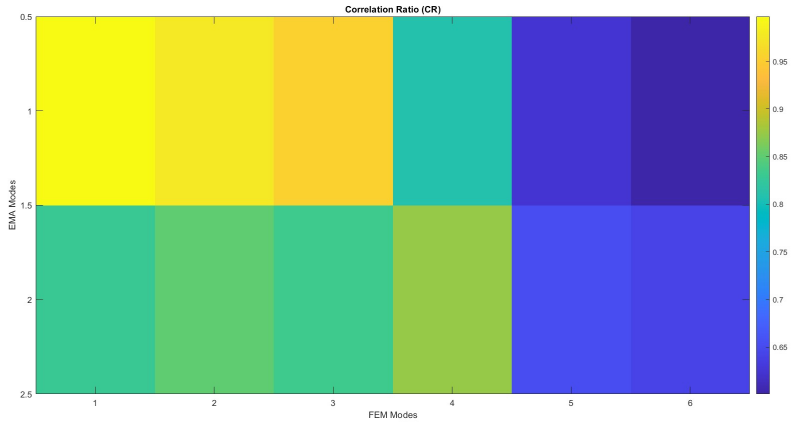

Figure 4.8: Heatmap illustrating the correlation metric between EMA and FEM modes.

One particularly notable observation is the strong similarity between **Mode 1 of EMA** and **Mode 6 of FEM**, which exhibit a correlation metric of 0.975. This high value reflects a strong agreement in the dynamic responses at the measured location. To further clarify this alignment, Figure 4.9 compares the normalized FRF magnitudes in

the X, Y, and Z directions for these modes.

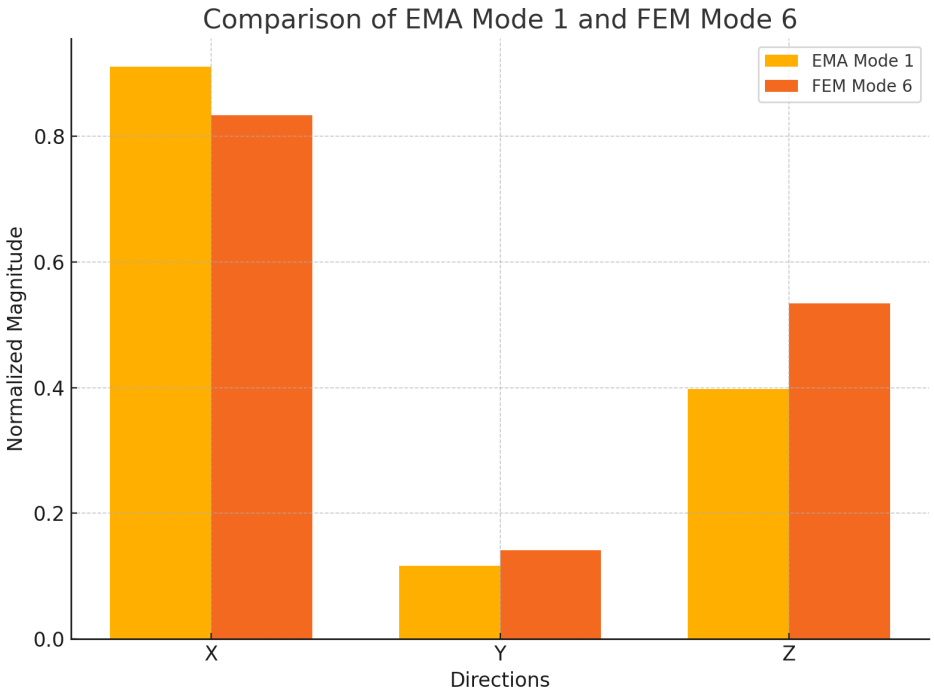

Figure 4.9: Comparison of normalized FRF magnitudes for EMA Mode 1 and FEM Mode 6 in the X, Y, and Z directions.

Frequency Analysis

The correlation metric findings are further substantiated by the frequency comparison. The natural frequency of Mode 1 from EMA was measured as 24.3 Hz, while the corresponding FEM mode (Mode 6) exhibited an undamped natural frequency of 22.519 Hz. The resulting frequency difference of 7.33% is well within acceptable bounds for engineering applications, affirming that the two modes represent the same physical phenomenon.

Conclusion

The results demonstrate a strong correlation between **Mode 1 of EMA** and **Mode 6 of FEM**, with a correlation metric of 0.975 and an acceptable frequency difference of 7.33%. While the approach does not involve full mode shapes, it offers a practical

means of evaluating modal similarity under the constraints of limited spatial data. The findings validate the FEM's capability to replicate the experimental dynamics of this mode and underscore the necessity of thorough data validation to ensure the robustness of the analysis.

4.3 Frequency Response Functions

4.3.1 EMA Analysis

The Frequency Response Functions (FRFs) obtained from Experimental Modal Analysis (EMA) are depicted in Figures 4.2 and 4.3. These FRFs are expressed as Acceleration-on-Force FRFs, a representation particularly advantageous for applications requiring sensitivity to high-frequency dynamics. High-frequency modes are critical in industries such as automotive and aerospace, where precision and stability hinge on capturing detailed dynamic behavior.

Acceleration-on-Force FRFs emphasize responses in higher frequency ranges due to the nature of acceleration measurements, enabling a focused analysis of dynamic behavior under high-frequency excitation. However, for a comprehensive understanding of structural deformation and its impact on stability, Displacement-on-Force FRFs are preferred. Displacement-based FRFs provide a direct insight into the structural response, highlighting resonance frequencies, dynamic compliance, and stiffness, which are vital for evaluating stability, particularly in low-frequency ranges where chatter typically occurs.

In this study, Acceleration-on-Force FRFs were transformed into Displacement-on-Force FRFs to enhance the interpretability of the results. This transformation accentuates low-frequency dynamics, allowing detailed examination of the structure's resonance behavior and stability. By leveraging the strengths of both representations, a balanced investigation of the dynamic performance across the frequency spectrum was achieved.

Displacement-on-Force FRFs

Figures 4.10 and 4.11 illustrate the Displacement-on-Force FRFs of the CNC machine tool in the X, Y, and Z directions, with force applied in the X and Y directions, respectively. These FRFs are instrumental for characterizing dynamic behavior, offering insights into resonance frequencies, stiffness, and compliance essential for machining stability analysis.

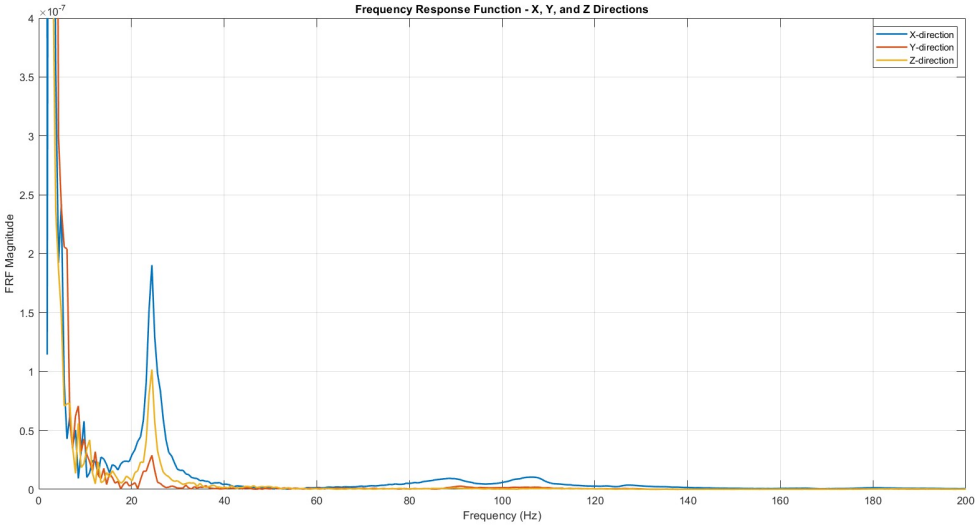

Figure 4.10: Displacement-on-Force Frequency Response Functions for the X, Y, and Z directions with force applied in the X direction.

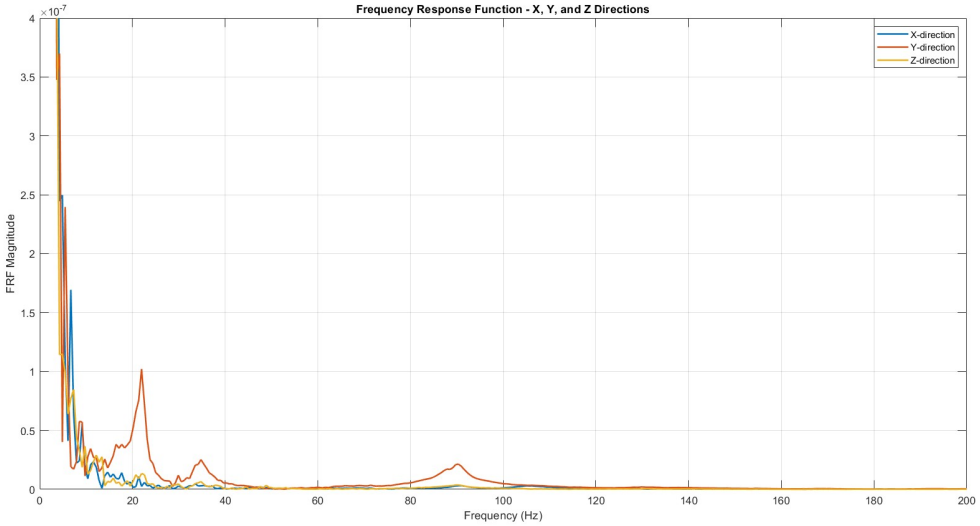

Figure 4.11: Displacement-on-Force Frequency Response Functions for the X, Y, and Z directions with force applied in the Y direction.

Observations from the FRFs

Force Applied in the X Direction

- **Prominent Resonance at 24.3 Hz:** A pronounced resonance peak in the X-direction FRF indicates significant dynamic compliance and reduced stiffness along this axis. The stronger response in the X direction, compared to Y and Z, highlights the structural anisotropy.
- **Responses in the Y and Z Directions:** Lower response magnitudes suggest higher stiffness and reduced compliance in these directions when force is applied along the X axis.

Force Applied in the Y Direction

- **Uniform Resonance Distribution:** Resonance peaks are smaller and more evenly distributed across all directions, reflecting balanced stiffness in the Y direction.

- **Dynamic Stiffness Variation:** Dynamic stiffness variation spreads more noticeably across all three directions, implying that the structure's compliance is more distributed when excited in the Y-direction and a more anisotropic response is evident when the force is applied in the Y-direction, potentially due to structural asymmetries.

Key Insights

- The X direction exhibits the highest compliance and pronounced resonance, whereas the Y direction demonstrates uniform stiffness with minimal resonance amplification.
- These characteristics are crucial for optimizing machining parameters to mitigate vibration-induced instabilities.

Chatter Analysis

Chatter, a critical concern in machining, is influenced by structural deformations that compromise stability. The analysis highlights significant resonance peaks in the lower frequency range, particularly around 24.3 Hz in the X direction, where the structure exhibits high compliance and reduced stiffness. This indicates a greater susceptibility to instability and chatter under typical operating conditions.

The machine tool demonstrates anisotropic behavior:

- The X direction shows pronounced resonance and lower stiffness, making it more vulnerable to chatter.
- The Y direction exhibits higher stiffness, resulting in reduced response magnitudes and greater stability against chatter.

These findings underscore the importance of optimizing machining parameters, such as spindle speed and depth of cut, to avoid critical resonance frequencies in the X direction. Structural enhancements, including improved stiffness along this axis, could further mitigate chatter and ensure stable machining performance.

4.3.2 FEM Analysis

Force Applied in the X Direction

The FEM-generated FRF for the X-direction shows a primary resonance peak around 20 Hz, indicating a structural mode with significant compliance in this direction. Additional smaller peaks are visible at approximately 40 Hz, 80 Hz, and 160 Hz, but their magnitudes are much lower, suggesting that the machine structure has a strong response primarily at lower frequencies when subjected to force in the X direction. This pattern implies that the structure has reduced stiffness along the X-axis compared to higher frequencies.

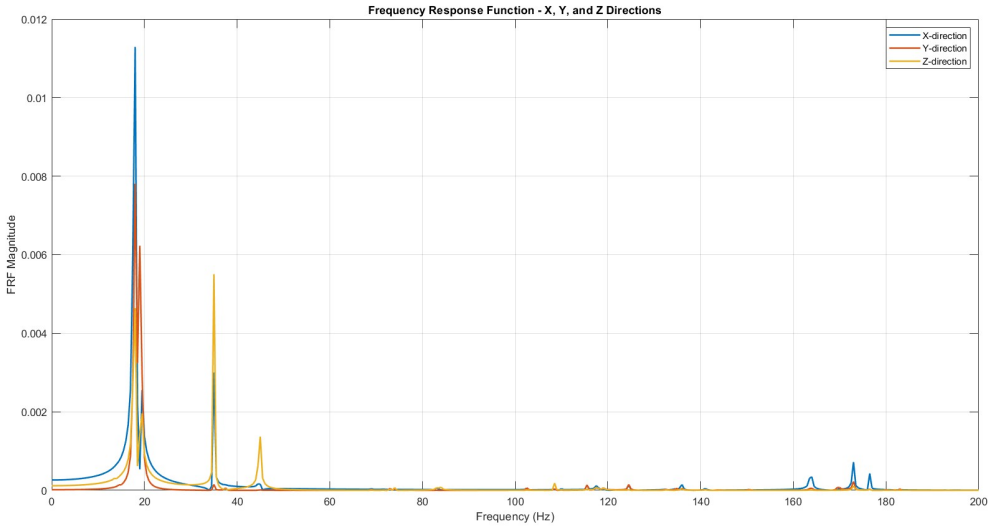

Figure 4.12: FEM-Generated FRFs with Force Applied in the X Direction

Force Applied in the Y Direction

Similarly, the Y-direction FEM-generated FRF displays a main resonance around 20 Hz, consistent with the X-direction, which indicates a fundamental mode at this frequency. Higher frequency peaks are also observed around 40 Hz, 80 Hz, and 160 Hz, but with even lower magnitudes compared to the X direction. This reduced response in the Y direction aligns with the machine's higher stiffness along the Y-axis, as seen in the

diminished response magnitude across all frequency ranges. This difference emphasizes the anisotropic stiffness properties of the machine tool.

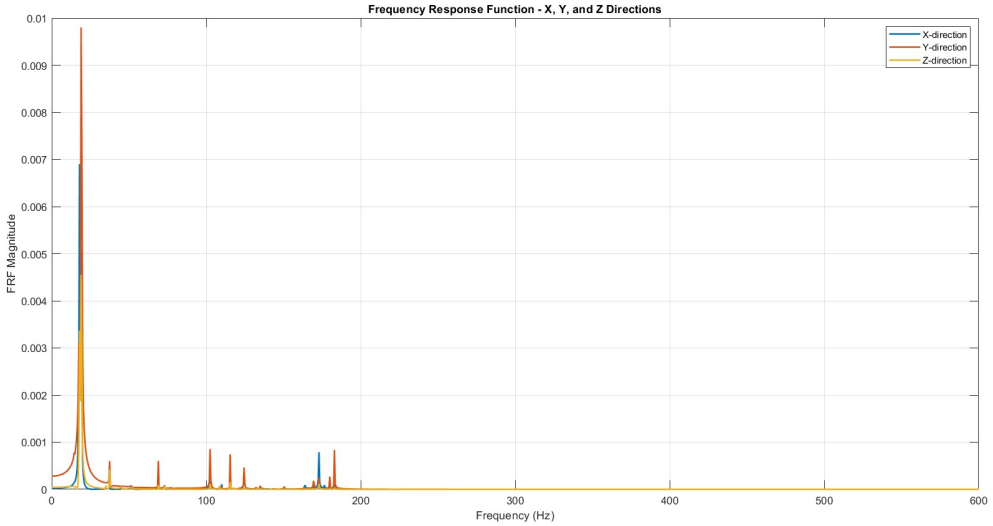

Figure 4.13: FEM-Generated FRFs with Force Applied in the Y Direction

4.3.3 Comparison of EMA and FEM Analyses

The dynamic characteristics of the CNC machine tool were assessed through Experimental Modal Analysis (EMA) and Finite Element Method (FEM) analysis. The key findings are summarized below:

- **Resonance Frequencies:**
  - **EMA:** The primary resonance was observed at **24.3 Hz** in the X direction, indicating significant compliance and susceptibility to chatter. In the Y direction, smaller and more distributed peaks confirmed higher stiffness.
  - **FEM:** The primary resonance was predicted at **22.5 Hz** for both X and Y directions, underestimating the experimental frequency by 24.3 Hz. Additional peaks at **40 Hz**, **80 Hz**, and **160 Hz** had significantly lower amplitudes.
- **Amplitudes and Compliance:**

  - Both analyses confirmed higher compliance in the X direction and greater stiffness in the Y direction.
  - **EMA:** Larger resonance amplitudes were observed, accurately representing real-world behavior.
  - **FEM:** Reduced amplitudes reflected idealized boundary conditions and simplified damping models.

- **Anisotropy:** Both methods identified anisotropic stiffness:
  - The X direction exhibited higher compliance and a greater risk of chatter.
  - The Y direction demonstrated higher stiffness and more stable dynamic behavior.

- **Practical Implications:**
  - **EMA:** Provides accurate insights into real-world dynamics, essential for optimizing machining parameters to avoid critical frequencies.
  - **FEM:** Useful for early-stage design but requires calibration with experimental data to improve accuracy in damping and high-frequency dynamics.

In conclusion, while FEM effectively predicts general stiffness characteristics, EMA is indispensable for accurate stability analysis due to its comprehensive representation of real-world dynamic responses.

4.4 Stability lobe diagrams

To evaluate and optimize the milling process, stability lobe diagrams have been generated using MillingStab software. These diagrams are essential for identifying stable cutting conditions, minimizing chatter, and ensuring efficient material removal. The input parameters required for this analysis have been meticulously determined based on both Experimental Modal Analysis (EMA) and the Finite Element Model (FEM).

A key aspect of this process is the choice of the CoroMill® 345 face milling cutter, selected specifically due to its suitability for power tests conducted during pre-acceptance and acceptance trials with customers. These tests are integral to verifying machine tool performance and compatibility with real-world machining conditions.

The input data includes results from power tests, material-specific properties for steel, and the technical specifications of the selected milling cutter (detailed in the Appendix). This comprehensive approach ensures the stability diagrams accurately reflect the dynamic behavior of the system, providing a reliable basis for process optimization. The subsequent sections will elaborate on the calculations and methodologies employed.

Table 4.2: CoroMill® 345 Face Milling Cutter Specifications

Specification	**Value**
Tool cutting edge angle (KAPR)	45 deg
Cutting diameter (DC)	100 mm
Maximum cutting diameter (DCX)	114.08 mm
Cutting item count (CICT_2)	5
Body material (BMC)	Steel

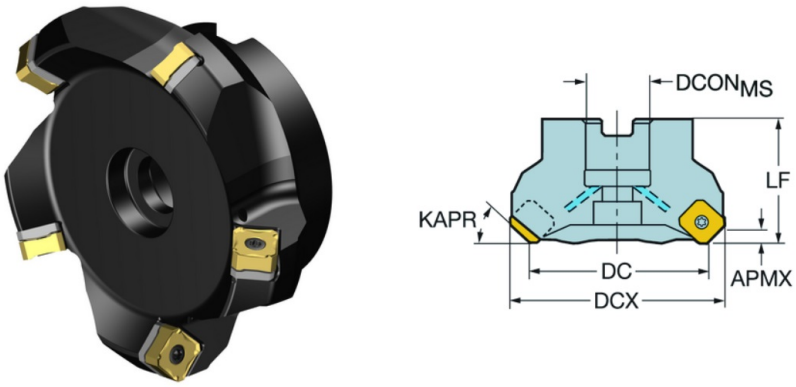

Figure 4.14: 345 Face Milling Cutter technical illustrations

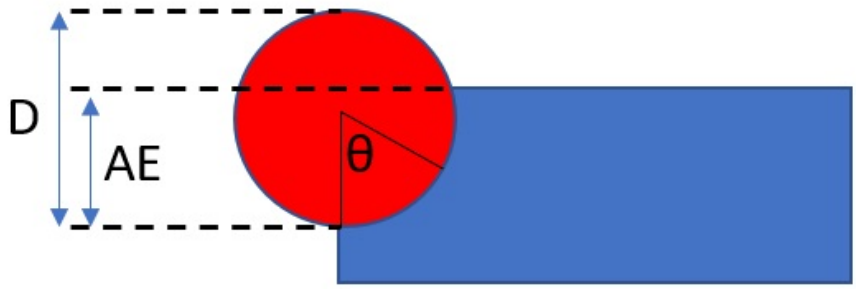

Figure 4.15: Illustration of radial depth of cut (AE) and engagement angle (θ) in milling

In milling operations, as illustrated in Figure 4.15, the engagement angle θ represents the angular portion of the tool in contact with the workpiece. This angle is calculated based on the tool diameter D and the radial depth of cut A_e. The equation

$$\theta = \arccos\left(\frac{r - A_e}{r}\right) = \arccos\left(\frac{D - 2A_e}{D}\right)$$

provides the engagement angle, which is crucial for analyzing cutting forces and assessing milling process stability.

For this analysis, the radial depth of cut is $A_e = 77.5\,\text{mm}$. Given the tool diameter $D = 100\,\text{mm}$, we calculate:

$$\theta = \arccos\left(\frac{100 - 2 \times 77.5}{100}\right) = 123.36^\circ$$

With this engagement angle, the start and exit angles entered into the MillingStab software are as follows:

- Start angle: $180^\circ - 123.36^\circ = 56.63^\circ$
- Exit angle: 180°

Additionally, for calculating the cutting force coefficients, we use the material coefficients for steel from machining handbooks. The tangential cutting force coefficient K_t and the radial cutting force coefficient K_r are given as $K_t = 3000\,\text{N/mm}^2$ and $K_r = 1200\,\text{N/mm}^2$, respectively. The axial cutting force coefficient K_{ac} can then be

determined from the initial radial cutting force coefficient K_{rc_0} and the inclination angle i using the equations:

$$K_{ac} = K_{rc_0} \cdot \tan(i)$$

$$K_{rc}(i) = \frac{K_{rc_0}}{\cos(i)}$$

where:

- K_{rc_0} is the initial radial cutting force coefficient.
- i is the inclination angle.

In our case, with an inclination angle $i = 0°$, there is no effect from the insert's tilt. Thus:

- $K_a = K_{rc_0} \cdot \tan(0°) = 1200 \cdot 0 = 0\,\mathrm{N/mm^2}$
- $K_r = \frac{K_{rc_0}}{\cos(0°)} = \frac{1200}{1} = 1200\,\mathrm{N/mm^2}$

Lastly, the angle K_i, which represents the lead angle δ, is specified as $K_i = 45°$ in this analysis.
Table 4.3 gathers all the calculated and input parameters needed for lobes diagram computation in the MillingStab software.

Table 4.3: Input Parameters for Lobes Diagram Computation

Parameter	**Value**	**Units**
Flutes Number	5	-
K_t	3000	$\mathrm{N/mm^2}$
K_r	1200	$\mathrm{N/mm^2}$
K_a	0	N/mm
K_i	45	degrees
Start Angle	56.63	degrees
Exit Angle	180	degrees
Rotation Direction	Clockwise	-

Figure 4.16: Input parameters entered in the MillingStab software for lobes diagram computation, including cutting force coefficients, start/exit angles, and rotation direction, with FRFs yet to be selected.

4.4.1 Analysis of Stability Lobe Diagrams Derived from EMA-Based FRFs

The stability lobe diagrams generated using the updated EMA-based FRFs illustrate how the dynamic behavior of the system changes with spindle speed and the applied frequency response configurations. The frequency range of interest remains **10–600 Hz**, ensuring high coherence. By exploring different combinations of FRFs—XX-XY, XX-YY, and YY-XY—the impact of cross-axis interactions and directional dynamics on stability is analyzed.

The **XX-XY FRF configuration** (Figure 4.17) combines the X-axis response to forces applied in both the X (XX) and Y (XY) directions. The updated stability lobe

diagram reveals fluctuating stability at lower spindle speeds, characterized by peaks and drops in the depth of cut. These fluctuations highlight the sensitivity of the system to cross-directional dynamics, making this configuration useful for analyzing systems with significant force-response coupling across axes.

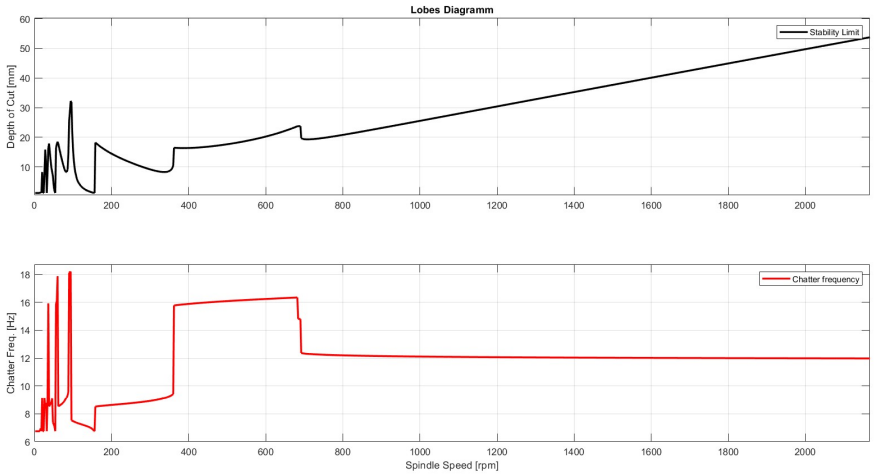

Figure 4.17: Stability Lobe Diagram with XX-XY FRFs (EMA-Based).

The **XX-YY FRF configuration** (Figure 4.18) measures responses in the X and Y directions corresponding to forces applied along the same axes. This configuration demonstrates a smoother stability trend compared to XX-XY, with depth of cut increasing consistently with spindle speed. The lack of cross-axis coupling results in more predictable stability behavior, suitable for applications requiring consistent stability across varying speeds.

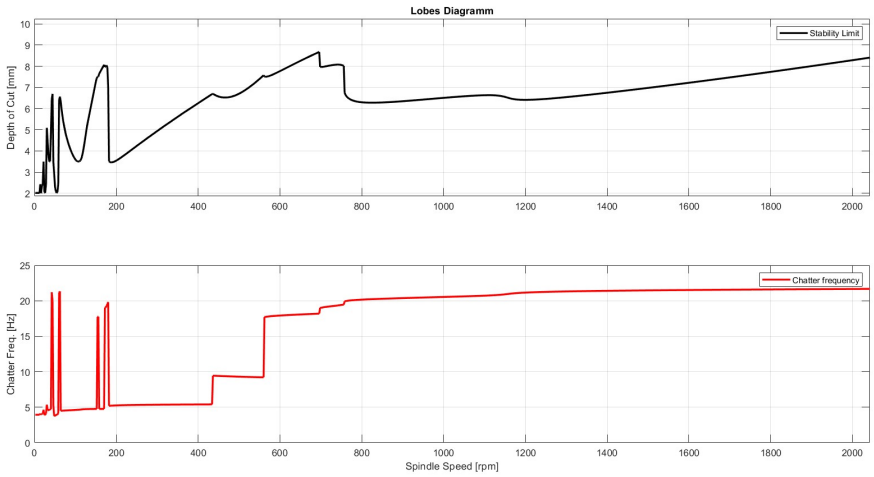

Figure 4.18: Stability Lobe Diagram with XX-YY FRFs (EMA-Based).

The **YY-XY FRF configuration** (Figure 4.19) highlights the sensitivity of the Y-axis response to both Y-applied forces (YY) and cross-axis forces (XY). The updated diagram shows distinct peaks at lower spindle speeds, similar to the XX-XY configuration but with a focus on Y-axis dynamics. This setup is especially valuable for evaluating lateral dynamics and cross-axis interactions in milling processes.

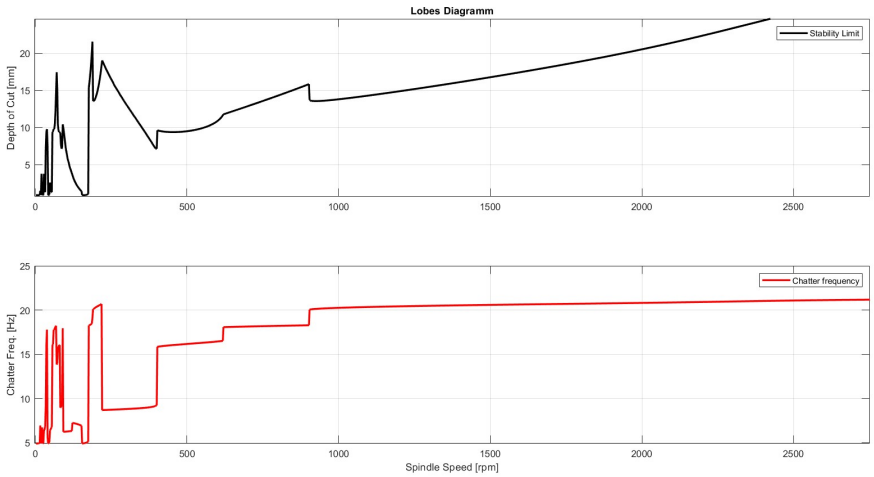

Figure 4.19: Updated Stability Lobe Diagram with YY-XY FRFs (EMA-Based).

4.4.2 Analysis of Stability Lobe Diagrams Derived from FEM-Based FRFs

The updated FEM-based stability lobe diagrams reflect the dynamic behavior of the system derived from computationally simulated FRFs over the same frequency range of **10–600 Hz**. The XX-XY, XX-YY, and YY-XY configurations provide insights into the influence of directional forces and responses.

The **XX-XY FRF configuration** (Figure 4.20) reveals significant fluctuations in stability at lower spindle speeds, with occasional high peaks in the depth of cut. These results indicate strong cross-directional effects due to Y-applied forces measured in the X direction. This configuration is critical for analyzing systems with substantial coupling between response directions.

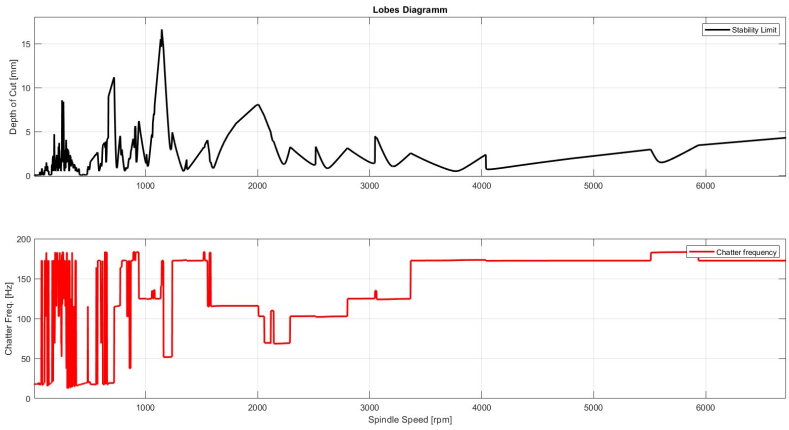

Figure 4.20: Updated Stability Lobe Diagram with XX-XY FRFs (FEM-Based).

The **XX-YY FRF configuration** (Figure 4.21) produces smoother trends, with stability limits increasing gradually as spindle speed rises. The absence of cross-directional coupling ensures consistent and predictable stability, ideal for applications requiring uniform behavior across a wide range of operational speeds.

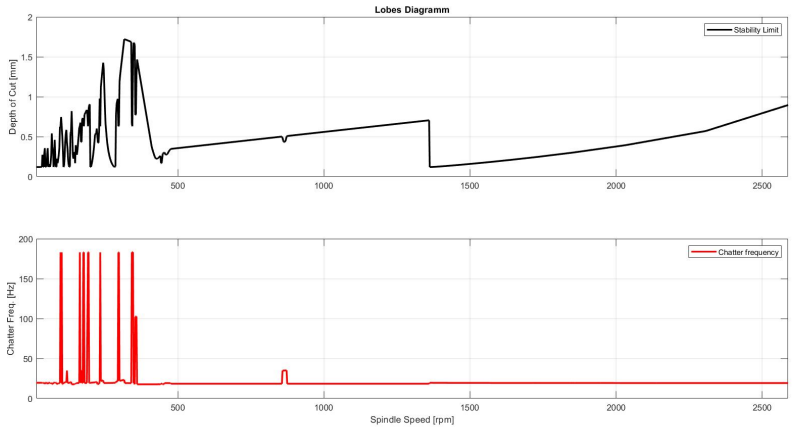

Figure 4.21: Updated Stability Lobe Diagram with XX-YY FRFs (FEM-Based).

The **YY-XY FRF configuration** (Figure 4.22) demonstrates peaks and irregular patterns at lower spindle speeds. The results emphasize the importance of Y-axis dynamics and cross-axis coupling introduced by Y-applied forces measured along the X direction. This configuration is valuable for understanding lateral dynamics and their influence on milling stability.

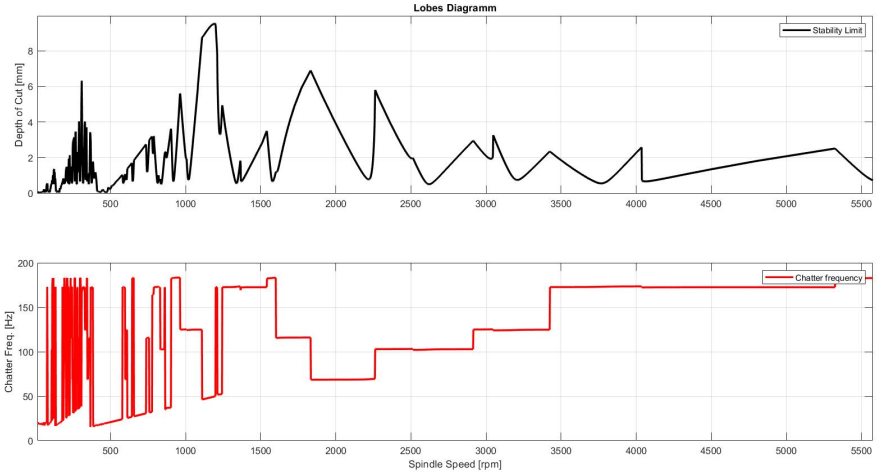

Figure 4.22: Updated Stability Lobe Diagram with YY-XY FRFs (FEM-Based).

4.4.3 Comparison of EMA and FEM Stability Lobe Diagrams

The updated diagrams highlight the differences between EMA and FEM approaches:

- **Stability Limits:** EMA results exhibit higher depth of cut values, influenced by real-world factors such as material damping, whereas FEM results predict lower limits due to idealized conditions.
- **Chatter Frequencies:** EMA demonstrates more variability at lower spindle speeds, capturing complex physical interactions, while FEM predictions are smoother and less sensitive to cross-axis effects.
- **Dynamic Sensitivity:** EMA reflects irregular patterns due to machine-tool interactions, while FEM offers a more consistent trend suitable for initial design studies.

Conclusion: EMA provides realistic insights into milling stability under operational conditions, whereas FEM offers computational efficiency for preliminary analysis. A combination of both methods enables robust predictions and design optimization.

Chapter 5

Conclusion and Future Works

5.1 Conclusion

This thesis has presented a comprehensive analysis of the dynamic behavior of CNC machine tools, specifically the Dynamill G5 gantry milling machine, through a combined approach involving Experimental Modal Analysis (EMA) and Finite Element Modeling (FEM). The study focused on structural responses, modal characteristics, and stability lobe diagrams to enhance chatter prediction and optimize machining performance.

The **Finite Element Model (FEM)**, developed in CATIA V5, effectively identified key resonance frequencies and mode shapes, demonstrating its utility for preliminary design and parameter studies. However, the FEM's inability to accurately capture damping effects and cross-axis dynamic interactions limited its predictive accuracy. FEM-derived stability lobe diagrams exhibited smoother trends with lower stability margins, reflecting the idealized assumptions in the model, such as uniform material properties and fixed boundary conditions.

The **Experimental Modal Analysis (EMA)** provided a more realistic depiction of the machine's dynamic behavior under operational conditions. Using impact testing and Frequency Response Function (FRF) analysis, EMA revealed the machine's anisotropic stiffness characteristics, with greater compliance in the X direction and increased stiffness

in the Y direction. Key resonance modes were identified at 24.3 Hz and 300.1 Hz, with damping ratios of $\zeta = 0.02$ and $\zeta = 0.01$, respectively. Stability lobe diagrams derived from EMA-based FRFs exhibited higher depth of cut limits, accurately reflecting real-world damping effects and machine-tool interactions.

The comparative analysis between EMA and FEM results highlighted the following key findings:

- **Resonance Frequencies:** FEM predicted the primary resonance at 22.5 Hz, while EMA identified it at 24.3 Hz, highlighting a 7.33% deviation attributed to idealized FEM assumptions.
- **Stability Limits:** EMA-based diagrams demonstrated higher depth of cut limits and more realistic stability predictions, incorporating damping and cross-axis interactions absent in FEM results.
- **Dynamic Behavior:** EMA captured complex machine-tool interactions and anisotropic stiffness, while FEM provided a smoother, computationally efficient representation of the system's dynamics.

The **MillingStab software** enabled the generation of stability lobe diagrams, providing insights into the impact of cross-axis dynamic interactions and FRF configurations (XX-XY, XX-YY, YY-XY). EMA-based FRFs produced superior stability margins, emphasizing the practical significance of experimental validation in dynamic stability analysis.

In conclusion, the integration of EMA and FEM offers a robust framework for dynamic analysis and machining stability evaluation. While FEM is valuable for initial design and optimization, EMA delivers critical insights into real-world performance, ensuring the reliability of stability predictions.

5.2 Future Works

Building on the findings of this study, several future research directions are proposed to refine and expand the methodologies:

1. Enhanced FEM Modeling

- Integrate experimentally derived parameters, such as damping ratios and material anisotropy, into the FEM to improve accuracy.
- Develop hybrid FEM-EMA models to capture higher-frequency dynamics and cross-axis coupling effects.
- Explore the influence of spindle-tool-holder dynamics and thermal effects on FEM predictions.

2. Extended Experimental Analysis

- Conduct multi-axis EMA to analyze coupled interactions between the X, Y, and Z directions, addressing limitations of single-axis testing.
- Investigate the impact of various tool-holder configurations and clamping conditions on damping and stability.
- Perform operational modal analysis during actual machining to evaluate the machine's in-process dynamics.

3. Advanced Stability Analysis

- Develop machine learning models to predict stability lobe diagrams under varying machining conditions, tool geometries, and materials.
- Study the influence of process damping at higher depths of cut and spindle speeds to expand the applicability of stability predictions.

4. Real-Time Monitoring and Control

- Design sensor-based systems for real-time monitoring of dynamic responses to enable adaptive control of spindle speed, depth of cut, and feed rate.
- Integrate auditory and vibration feedback for in-process chatter detection and operator training.

5. Validation Through Industrial Case Studies

- Conduct systematic milling experiments under varying cutting conditions to validate and generalize the findings.
- Extend the proposed methodologies to other CNC machine tools and machining processes, such as turning and drilling.

6. Sustainability Integration

- Evaluate the energy efficiency of stability-enhancing modifications to align with sustainable manufacturing practices.
- Explore the use of lightweight and high-damping materials for machine components to improve dynamic stability while reducing energy consumption.

By addressing these areas, future research can further enhance the integration of EMA and FEM, enabling more accurate, reliable, and sustainable predictions of machining stability and performance.

Chapter 6

Appendix

Table 6.1: ICP® Impact Hammer Specifications (Model TLD086C04)

SPECIFICATIONS		
	ENGLISH	**SI**
PERFORMANCE		
Sensitivity (±15%)	5 mV/lbf	1.1 mV/N
Measurement Range	±1000 lbf pk	±4448 N pk
Resonant Frequency	≥22 kHz	≥22 kHz
Non-Linearity	≤ 1%	≤ 1%
ELECTRICAL		
Excitation Voltage	20 to 30 VDC	20 to 30 VDC
Constant Current Excitation	2 to 20 mA	2 to 20 mA
Output Impedance	< 100 Ohm	< 100 Ohm
Output Bias Voltage	8 to 14 VDC	8 to 14 VDC
Discharge Time Constant	≥2000 sec	≥2000 sec
PHYSICAL		
Sensing Element	Quartz	Quartz
Sealing	Epoxy	Epoxy
Hammer Mass	0.34 lb	0.16 kg
Head Diameter	0.62 in	1.57 cm
Tip Diameter	0.25 in	0.63 cm
Hammer Length	8.5 in	21.6 cm
Electrical Connection Position	Bottom of Handle	Bottom of Handle
Extender Mass Weight	2.6 oz	75 gm
Electrical Connector	BNC Jack	BNC Jack

Table 6.2: Triaxial ICP® Accelerometer Specifications (Model 356A45)

SPECIFICATIONS		
	ENGLISH	**SI**
PERFORMANCE		
Sensitivity (±10%)	100 mV/g	10.2 mV/(m/s^2)
Measurement Range	±50 g pk	±490 m/s^2 pk
Frequency Range (±5%)	0.7 to 7000 Hz	0.7 to 7000 Hz
Frequency Range (±10%)	0.4 to 10000 Hz	0.4 to 10000 Hz
Resonant Frequency	≥30 kHz	≥30 kHz
Broadband Resolution (1)	0.0005 g rms	0.005 m/s^2 rms
Non-Linearity	≤ 1%	≤ 1%
Transverse Sensitivity	≤ 6%	≤ 6%
ENVIRONMENTAL		
Overload Limit (Shock)	±5000 g pk	±49050 m/s^2 pk
Temperature Range (Operating)	-65 to 185 °F	-54 to 85 °C
Base Strain Sensitivity	0.001 g/$\mu\epsilon$	0.01 (m/s^2)/$\mu\epsilon$
ELECTRICAL		
Excitation Voltage	20 to 30 VDC	20 to 30 VDC
Constant Current Excitation	2 to 20 mA	2 to 20 mA
Output Impedance	≤200 Ohm	≤200 Ohm
Output Bias Voltage	8 to 12 VDC	8 to 12 VDC
Discharge Time Constant	0.8 to 2.4 sec	0.8 to 2.4 sec
Settling Time	≤5 sec	≤5 sec
Spectral Noise (1 Hz)	125 $\mu g/\sqrt{\text{Hz}}$	1226 (μm/s^2)/$\sqrt{\text{Hz}}$
Spectral Noise (10 Hz)	40 $\mu g/\sqrt{\text{Hz}}$	392 (μm/s^2)/$\sqrt{\text{Hz}}$
Spectral Noise (100 Hz)	15 $\mu g/\sqrt{\text{Hz}}$	147 (μm/s^2)/$\sqrt{\text{Hz}}$
Spectral Noise (1 kHz)	4 $\mu g/\sqrt{\text{Hz}}$	39.2 (μm/s^2)/$\sqrt{\text{Hz}}$
PHYSICAL		
Sensing Element	Ceramic	Ceramic
Sensing Geometry	Shear	Shear
Housing Material	Titanium	Titanium
Sealing	Hermetic	Hermetic
Size - Height	0.40 in	10.2 mm
Size - Length	0.75 in	19.1 mm
Size - Width	0.40 in	10.2 mm
Weight	0.15 oz	4.2 gm
Electrical Connector	1/4-28 4-Pin	1/4-28 4-Pin
Mounting	Adhesive	Adhesive

Table 6.3: CoroMill® 345 Face Milling Cutter Specifications

Specification	**Value**
Tool cutting edge angle (KAPR)	45 deg
Cutting diameter (DC)	100 mm
Maximum cutting diameter (DCX)	114.08 mm
Cutting item count (CICT_2)	5
Part 2 of cutting item interface identifiers (CUTINT_MASTER_2)	CoroMill 345 - size 1305 (345R-1305)
Clamping type code (MTP)	clamp with screw through hole
Depth of cut maximum (APMX_FFW)	6 mm
Maximum ramping angle (RMPX)	0 deg
Maximum plunge depth (AZ)	0 mm
Cutting pitch differential (CPDF)	Yes
Peripheral effective cutting edge count (ZEFP)	5
Connection - machine side (ADINTMS)	Arbor -ISO 6462 -A (hexagon socket head cap screw) -metric: 32
Hand (HAND)	Right
Coolant entry style (CNSC)	axial concentric entry
Coolant pressure (CP)	10 bar
Connection diameter machine side (DCONMS)	32 mm
Standard number (STDNO)	ISO6462
Standard letter (STDLET)	A
Functional length (LF)	50 mm
Radial rake angle (GAMF)	-12.7324 deg
Axial rake angle (GAMP)	-4.5631 deg
Torque (TQ)	3 Nm
Body material (BMC)	Steel
Rotational speed maximum (RPMX)	12,200 1/min
Weight of item (WT)	1.875 kg
Release date (ValFrom20)	10/02/2009
Release pack id (RELEASEPACK)	09.1

Bibliography

[1] Vincent Moreau. Dynamic study of machining and tool-part interaction using displacement measurement: application for milling and turning operation. 01 2010.

[2] R. Patel. Study on the influence of helix angle and radial immersion on forced vibrations in milling. *International Journal of Machine Tools and Manufacture*, 48(5):367–374, 2008.

[3] M. Campomanes and R. Salgado. Effect of cutting parameters on forced vibration in milling operations. *Journal of Manufacturing Science and Engineering*, 125(3):475–481, 2003.

[4] G. Peigné and E. Duc. Investigation of vibration in interrupted machining processes. *Journal of Materials Processing Technology*, 142(3):676–683, 2003.

[5] P. Albrecht and N. Sahni. Sources of forced vibrations in high-speed milling. *CIRP Annals - Manufacturing Technology*, 54(1):407–410, 2005.

[6] T. L. Schmitz. Effect of runout and imbalance on surface quality in high-speed milling. *Precision Engineering*, 31(1):35–41, 2007.

[7] W. Jeong and D. A. Dornfeld. Study of workpiece deformation in turning operations. *Journal of Manufacturing Processes*, 7(2):95–104, 2005.

[8] R. N. Arnold. The mechanism of tool vibration in the cutting of steel. *Proceedings of the Institution of Mechanical Engineers*, 154:261–284, 1946.

[9] J. Tlusty and M. Polacek. The stability of machine tools against self-excited vibrations in machining. *International Research in Production Engineering*, pages 465–474, 1963.

[10] H. E. Merritt. Theory of self-excited machine tool chatter. *Journal of Engineering for Industry*, 87(4):447–454, 1965.

[11] S. A. Tobias. *Machine-Tool Vibration*. Blackie and Sons Ltd., London, 1965.

[12] M. Zhao and B. Balachandran. Dynamics and stability of milling process. *International Journal of Solids and Structures*, 38(10-13):2233–2248, 2001.

[13] J. Tlusty. Dynamics of High-Speed Milling. *Journal of Engineering for Industry*, 108(2):59–67, 05 1986.

[14] Y. Altintaş and E. Budak. Analytical prediction of stability lobes in milling. *CIRP Annals*, 44(1):357–362, 1995.

[15] Yuzhong Cao and Y. Altintas. Modeling of spindle-bearing and machine tool systems for virtual simulation of milling operations. *International Journal of Machine Tools and Manufacture*, 47(9):1342–1350, 2007. Selected papers from the 2nd International Conference on High Performance Cutting.

[16] Huseyin Celikag, Erdem Ozturk, and Neil D. Sims. Can mode coupling chatter happen in milling? *International Journal of Machine Tools and Manufacture*, 165:103738, 2021.

[17] Kasper Ringgaard, Nikolaj Knudsen, Jens Jensen, Martin Ørum Ørhem Juul, and Ole Balling. Characterization of machine tool vise using operational modal analysis. *Procedia CIRP*, 82:249–254, 2019. 17th CIRP Conference on Modelling of Machining Operations (17th CIRP CMMO).

[18] Y. Altintas, G. Stepan, D. Merdol, and Z. Dombovari. Chatter stability of milling in frequency and discrete time domain. *CIRP Journal of Manufacturing Science and Technology*, 1(1):35–44, 2008.